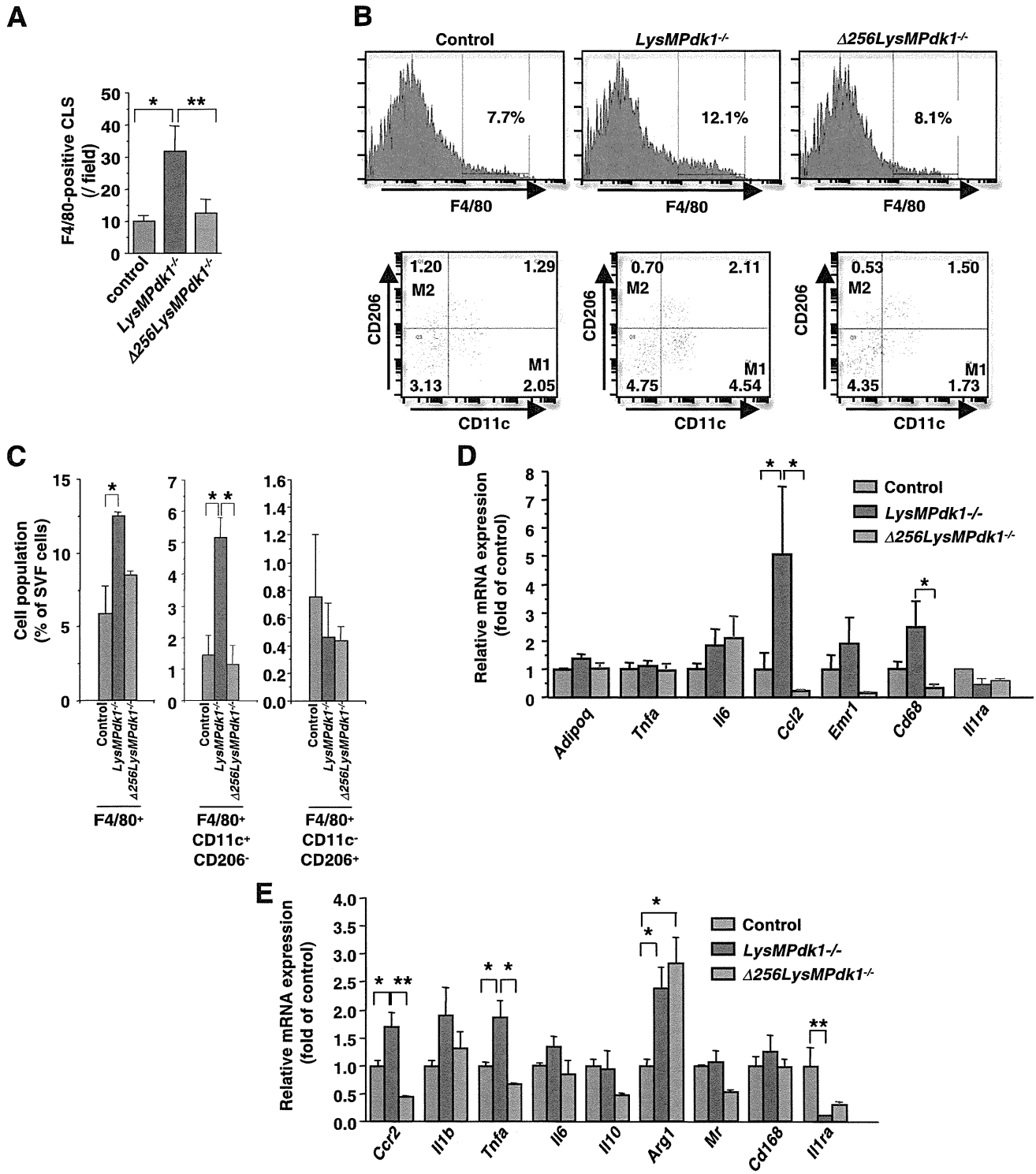

FIG. 3. Effects of *Pdk1* deletion or inhibition of the transactivation of Foxo1 on adipose tissue inflammation. *A*: CLSs in epididymal fats were quantified from eight different fields per mouse and presented as number of CLSs per field. Data are means + SEM of 9–10 mice in each genotype. $^*P < 0.01$ (one-factor ANOVA of *LysMPdk1*$^{-/-}$ vs. control mice) and $^{**}P < 0.05$ (one-factor ANOVA of *LysMPdk1*$^{-/-}$ vs. *Δ256LysMPdk1*$^{-/-}$ mice). *B*: The expression of F4/80 and CD11c and CD206 in the SVF of epididymal fat from 20- to 24-week-old mice of the indicated genotype as assessed by flow cytometry. *C*: The percentages of F4/80$^+$, F4/80$^+$CD11c$^+$CD206$^-$, and F4/80$^+$CD11c$^-$CD206$^+$ cells within the viable SVF from 20- to 24-week-old mice of control, *LysMPdk1*$^{-/-}$, and *Δ256LysMPdk1*$^{-/-}$ mice. Data are means + SEM of three mice in each genotype analyzed in three independent experiments. $^*P < 0.05$ (one-factor ANOVA of *LysMPdk1*$^{-/-}$ vs. control or *Δ256LysMPdk1*$^{-/-}$ mice). *D*: Expression of genes in the epididymal fat of control, *LysMPdk1*$^{-/-}$, and *Δ256LysMPdk1*$^{-/-}$ mice. Values were normalized to β-actin expression and represent the means + SEM of 8–10 mice per genotype. $^*P < 0.05$ (one-factor ANOVA). *E*: Expression of genes specific for M1 (*Ccr2*, *Il1b*, *Tnfa*, and *Il6*) or M2 (*Il10*, *Arg1*, *Mr*, and *Cd168*) macrophage in SVF of epididymal fat in control, *LysMPdk1*$^{-/-}$, and *Δ256LysMPdk1*$^{-/-}$ mice. Values were normalized to β-actin expression and represent the means + SEM of 8–10 mice per genotype. $^*P < 0.05$ and $^{**}P < 0.01$ (one-factor ANOVA).

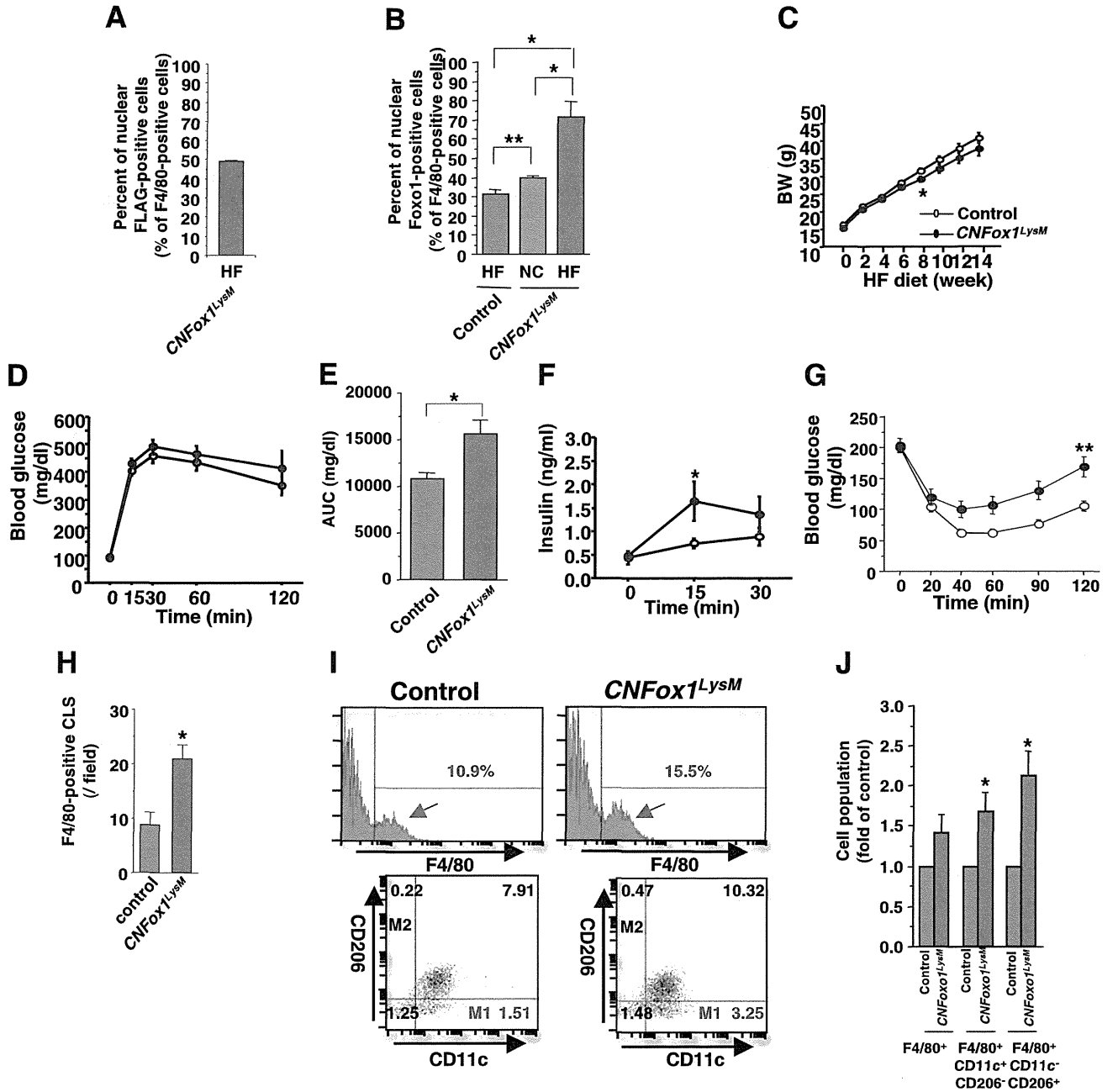

FIG. 4. Effects of the overexpression of CNFoxo1 in macrophages on glucose metabolism and adipose tissue inflammation. *A*: The percentages of nuclear FLAG$^+$ among F4/80$^+$ cells in epididymal fat of *CNFoxo1*^{LysM} fed an HFD for 16 weeks. Counting of cells stained with anti-FLAG and anti-F4/80 are described in RESEARCH DESIGN AND METHODS. *B*: The percentages of nuclear Foxo1$^+$ among F4/80$^+$ cells in epididymal fat of control, *CNFoxo1*^{LysM} fed an NC, and *CNFoxo1*^{LysM} mice aged 20 weeks and fed an HFD for 16 weeks. Counting of cells stained with anti-F4/80 and anti-FOXO1 are described in RESEARCH DESIGN AND METHODS. Values are means + SEM of eight mice in each genotype. *$P < 0.005$ and **$P < 0.05$ (one-factor ANOVA). *C*: Body weight (BW) of control and *CNFoxo1*^{LysM} mice fed an HFD. Data are means + SEM of 18–20 mice in each genotype. *$P < 0.05$ (two-way repeated-measures ANOVA with an ad hoc multiple comparison method [Fisher LSD test] of control vs. *CNFoxo1*^{LysM} mice after 8 weeks of HFD). *D*: IPGTT of control (open circle) and *CNFoxo1*^{LysM} (blue circle) mice fed an HFD. Data are means + SEM of 20–25 mice in each genotype. *E*: Comparison of AUC in control and *CNFoxo1*^{LysM} mice during IPGTT. Data are means + SEM of 20–25 mice in each genotype. *$P < 0.05$ (two-way repeated-measures ANOVA with Fisher LSD test of control vs. *CNFoxo1*^{LysM} mice). *F*: Insulin secretion of control (open circle) and *CNFoxo1*^{LysM} (blue circle) mice during IPGTT. Data are means + SEM of 20–25 mice in each genotype. *$P < 0.05$ (two-way repeated-measures ANOVA with Fisher LSD test of control vs. *CNFoxo1*^{LysM} mice). *G*: ITT of control (open circle) and *CNFoxo1*^{LysM} (blue circle) mice. Data are means + SEM of 20–25 mice in each genotype. *$P < 0.01$ and **$P < 0.05$ (two-way repeated-measures ANOVA with Fisher LSD test of control vs. *CNFoxo1*^{LysM} mice). *H*: CLSs in epididymal fats were quantified from eight different fields per mouse and presented as number of CLSs per field. Data are means + SEM of 9–10 mice in each genotype. *$P < 0.05$ (one-factor ANOVA of control vs. *CNFoxo1*^{LysM} mice). *I*: Expression of F4/80 and CD11c and CD206 in cells of the SVF of epididymal fat from control and *CNFoxo1*^{LysM} mice fed an HFD for 16 weeks as assessed by flow cytometry. *J*: The percentages of F4/80$^+$, F4/80$^+$CD11c$^+$CD206$^-$, and F4/80$^+$CD11c$^-$CD206$^+$ cells within the viable SVF from control and *CNFoxo1*^{LysM} 20- to 24-week-old mice fed an HFD for 16 weeks. The percentages of cell population among total SVF cells were calculated in each experiment. Data are means + SEM of fold change of control mice in each genotype ($n = 3$) analyzed in three independent experiments. *$P < 0.05$ (one-factor ANOVA of control vs. *CNFoxo1*^{LysM} mice).

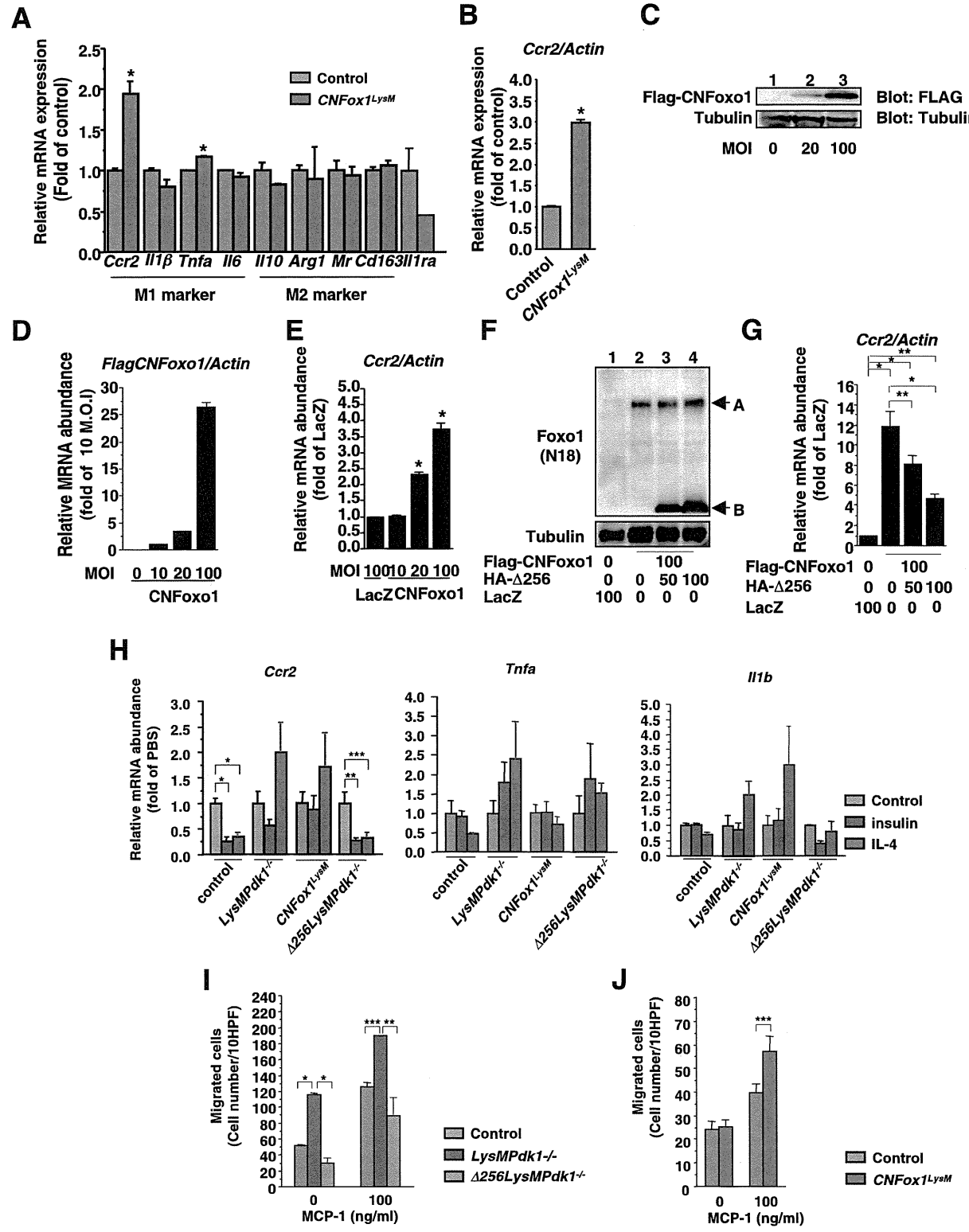

FIG. 5. Foxo1 increases migration capacity by inducing *Ccr2* expression. *A*: Expression of genes specific for M1 (*Ccr2*, *Il1b*, *Tnfa*, and *Il6*) or M2 (*Il10*, *Arg1*, *Mr*, and *Cd168*) phenotype of cells of the SVF from control and *CNFoxo1*^{LysM} mice fed an HFD for 16 weeks. Values were normalized to β-actin expression and represent the means + SEM of 8–10 mice per genotype. *$P < 0.05$ (one-factor ANOVA of control vs. *CNFoxo1*^{LysM} mice). *B*: Expression of *Ccr2* in ATMs sorted from the SVF of epididymal fat from control and *CNFoxo1*^{LysM} mice fed an HFD for 16 weeks. Values were normalized to β-actin expression and represent the means + SEM of three mice per genotype. *$P < 0.05$ (one-factor ANOVA of control vs. *CNFoxo1*^{LysM} mice). *C*: Flag-CNFoxo1 protein expression was detected in RAW264.7 cells. Nontransduced RAW264.7 cells (*lane 1*); RAW264.7 cells transduced with adenovirus encoding CNFoxo1 at 20 and 100 MOI (*lanes 2* and *3*, respectively). Western blot of cell lysates using anti-tubulin antibody (*bottom*). *D*: Expression of *Flag-CNFoxo1* gene in RAW264.7 cells transduced with adenoviruses encoding CNFoxo1 at the indicated MOI. *E*: Real-time PCR to determine *Ccr2* expression in RAW264.7 cells transduced with adenovirus encoding LacZ or CNFoxO1 at the indicated

and tissue weights of *CNFoxo1*^{LysM} mice were similar to those of control mice. However, adipocyte size in the epididymal fat of *CNFoxo1*^{LysM} mice tended to be larger than that in control mice (Fig. 4*C* and Supplementary Fig. 8*A–C*). Although, on the HFD, *CNFoxo1*^{LysM} and control mice exhibited similar glucose tolerance (Fig. 4*D*), the AUC of the IPGTT was significantly increased in *CNFoxo1*^{LysM} compared with control mice (Fig. 4*E*). Furthermore, the *CNFoxo1*^{LysM} mice exhibited significantly increased insulin secretion and decreased insulin sensitivity (Fig. 4*F* and *G*). These data suggest that the CNFoxo1 in ATMs caused insulin resistance.

M1 macrophage population was increased in *CNFoxo1*^{LysM} mice. Adipocyte size and CLS density exhibit a positive correlation (32,36). Indeed, under HFD conditions, *CNFoxo1*^{LysM} mice had a significantly higher number of CLSs in epididymal fat than control mice (Fig. 4*H*). Phenotypic analysis of ATMs revealed significantly more F4/80$^+$ cells in the SVF of *CNFoxo1*^{LysM} mice compared with control mice (Fig. 4*I* and *J*). Further analysis showed that *CNFoxo1*^{LysM} mice had a significantly higher percentage of F4/80$^+$CD11c$^+$CD206$^-$ and F4/80$^+$CD11c$^-$CD206$^+$ cells compared with control mice (Fig. 4*I* and *J*). These data suggest that the *CNFoxo1*^{LysM} mice have increased numbers of macrophages in adipose tissues under HFD conditions.

CNFoxo1-induced *Ccr2* gene expression. To investigate how CNFoxo1 increased the M1 macrophage subpopulation in adipose tissue, we analyzed gene expression in the SVF of epididymal fat from mice fed an HFD. Real-time PCR demonstrated that *CNFoxo1*^{LysM} mice expressed significantly higher levels of *Ccr2* and *Tnfa* mRNAs than control mice (Fig. 5*A*). Furthermore, the level of *Ccr2* expression in F4/80$^+$CD11c$^+$CD206$^-$ cells was significantly increased in *CNFoxo1*^{LysM} mice compared with control mice (Fig. 5*B*). To examine whether CNFoxo1 directly induces *Ccr2* expression, we infected RAW264.7 cells with an adenovirus encoding β-galactosidase or CNFoxo1. Overexpression of CNFoxo1 in RAW264.7 cells significantly increased endogenous *Ccr2* expression (Fig. 5*C–E*). These data suggest that the overexpression of CNFoxo1 in ATMs increased *Ccr2* expression.

Next, we investigated whether Δ256Foxo1 could block Foxo1-induced *Ccr2* expression. We cotransduced RAW264.7 cells with adenoviruses that encoded Flag-CNFoxo1 and HA-Δ256Foxo1. We found that the presence of Δ256Foxo1 inhibited the expression of endogenous *Ccr2* in a dose-dependent manner (Fig. 5*F* and *G*). These data indicate and confirm that the Δ256Foxo1 construct had a dominant negative effect on Foxo1-induced *Ccr2* expression.

Insulin- and IL-4–inhibited *Ccr2* gene expression. To determine whether Foxo1 regulation of *Ccr2* expression was involved in insulin signaling, we tested whether insulin or IL-4 inhibited *Ccr2* expression in a Foxo1-dependent manner. Both insulin and IL-4 could significantly inhibit *Ccr2* expression in BMDMs from control and *Δ256LysMPdk1*$^{-/-}$ mice but not in BMDMs from *LysMPdk1*$^{-/-}$ and *CNFoxo1*^{LysM} mice (Fig. 5*H*). In contrast, insulin and IL-4 did not affect expression of other genes specifically expressed in M1 macrophages, including *Tnfa* and *Il1b* (Fig. 5*H*). These data indicate that Foxo1-induced *Ccr2* expression was regulated by both insulin and IL-4.

Pdk1 deletion or CNFoxo1 expression enhanced macrophage migration. To analyze the functional effects of Pdk1 deficiency in macrophages, we performed transwell migration assays with BMDMs. Pdk1-deficient BMDMs exhibited significantly more migration than BMDMs from control and *Δ256LysMPdk1*$^{-/-}$ mice (Fig. 5*I*). Furthermore, BMDMs from *CNFoxo1*^{LysM} mice exhibited significantly increased MCP-1–stimulated migration capacity compared with control BMDMs (Fig. 5*J*). These data confirm that a Pdk1 deficiency and/or Foxo1 activation in macrophages resulted in increased migration as a result of increased expression of Ccr2.

Characterization of the Foxo1 response element within the *Ccr2* promoter. To characterize the Foxo1 response element (FRE) in the *Ccr2* promoter, we constructed different versions of the mouse *Ccr2* promoter by progressively deleting portions of the upstream region. The transcriptional activity of each mutant promoter in response to CNFoxo1 binding was examined in HEK293T cells (Fig. 6*A*). *Ccr2* promoters with deletions up to −291 nucleotides (nt) responded to Foxo1 transactivation. However, further deletions, up to −208 nt, completely abolished transcription of the reporter (Fig. 6*A*). Thus, the FRE was confined to a small nucleotide region between −291 and −208 in the mouse *Ccr2* promoter. Consistent with this observation, the promoter region contained several putative Foxo response elements (FREs), including GTAAAT from −254 to −249 nt and AAACA from −215 to −211 nt (Fig. 6*A*). It is interesting that the former region is conserved among human, mouse, and rat *Ccr2* promoters (Supplementary Fig. 9). To confirm this finding, we generated one additional truncated mutant promoter (237Ccr2), which had the latter FRE but not the former. The 237*Ccr2* promoter did not respond to Foxo1 induction. These data suggest that the AAACA sequence from −215 to −211 was unnecessary for Foxo1 activation of the *Ccr2* promoter. We also generated two additional mutant *Ccr2* promoters, one harboring nucleotide substitutions between −254 and −249 (254mut) and one with substitutions between −215 and −211 (215mut). Foxo1 induced transcription from the 215mut but not from the 254mut *Ccr2* promoter (Fig. 6*A*). These data suggest that the GTAAAT

MOI. The cells were transduced, incubated in complete medium, and harvested 48 h after transduction. Data (mean ± SEM) are from three independent experiments and normalized to the amount of β-actin mRNA, expressed as relative to the corresponding LacZ value. *$P < 0.05$ (one-factor ANOVA of cells transduced with LacZ vs. CNFoxo1 at 20 or 100 MOI). *F*: Expression of Flag CNFoxO1 and HA-Δ256FoxO1 at indicated MOI in RAW264.7 cells. Western blot using anti-Foxo1 (N18) antibody, which recognizes the NH_2 terminus of Foxo1 (*top*). Arrows A and B indicate Flag-CNFoxo1 and HA-Δ256Foxo1, respectively. *G*: The effects of HA-Δ256Foxo1 on Flag-CNFoxo1–induced *Ccr2* expression in RAW264.7 cells. Data are means + SEM from three independent experiments and are expressed as the fold change from endogenous *Ccr2* expression in RAW264.7 cells transduced with an adenovirus encoding LacZ. *$P < 0.005$ and **$P < 0.05$ (one-factor ANOVA of cells transduced with LacZ vs. Flag-CNFoxo1 at MOI 100 and cells transduced with Flag-CNFoxo1 at MOI 100 vs. HA-Δ256Foxo1 at MOI 50 and 100). *H*: Expression of genes *Ccr2*, *Tnfa*, and *Il1b* of BMDM from the indicated genotypes. Cells were cultured for 6 days in the presence of PBS, insulin (100 nmol/L), or IL-4 (100 ng/mL). Values were normalized to β-actin expression and represent the means + SEM of fold of PBS in each genotype (8–10 mice per genotype). *$P < 0.005$ (one-factor ANOVA of PBS vs. insulin or IL-4 in control mice), **$P < 0.01$ (one-factor ANOVA of PBS vs. insulin in *Δ256LysMPdk1*$^{-/-}$ mice), and ***$P < 0.05$ (one-factor ANOVA of PBS vs. IL-4 in *Δ256LysMPdk1*$^{-/-}$ mice). *I* and *J*: Migration of BMDM from control, *LysMPdk1*$^{-/-}$, and *Δ256LysMPdk1*$^{-/-}$ mice (*I*) and from control and *CNFoxo1*^{LysM} mice (*J*) through a gelatin matrix was analyzed using a transwell migration assay at the indicated concentration of MCP-1. Data are means + SEM of cell numbers per 10 high power fields (HPFs) from three independent experiments. *$P < 0.005$ (one-factor ANOVA of *LysMPdk1*$^{-/-}$ vs. control or *Δ256LysMPdk1*$^{-/-}$ mice at basal condition), **$P < 0.01$ (one-factor ANOVA of *LysMPdk1*$^{-/-}$ vs. *Δ256LysMPdk1*$^{-/-}$ mice at 100 ng/mL of MCP-1), and ***$P < 0.05$ (one-factor ANOVA of *LysMPdk1*$^{-/-}$ vs. control mice and of control vs. *CNFoxo1*^{LysM} mice at 100 ng/mL of MCP-1).

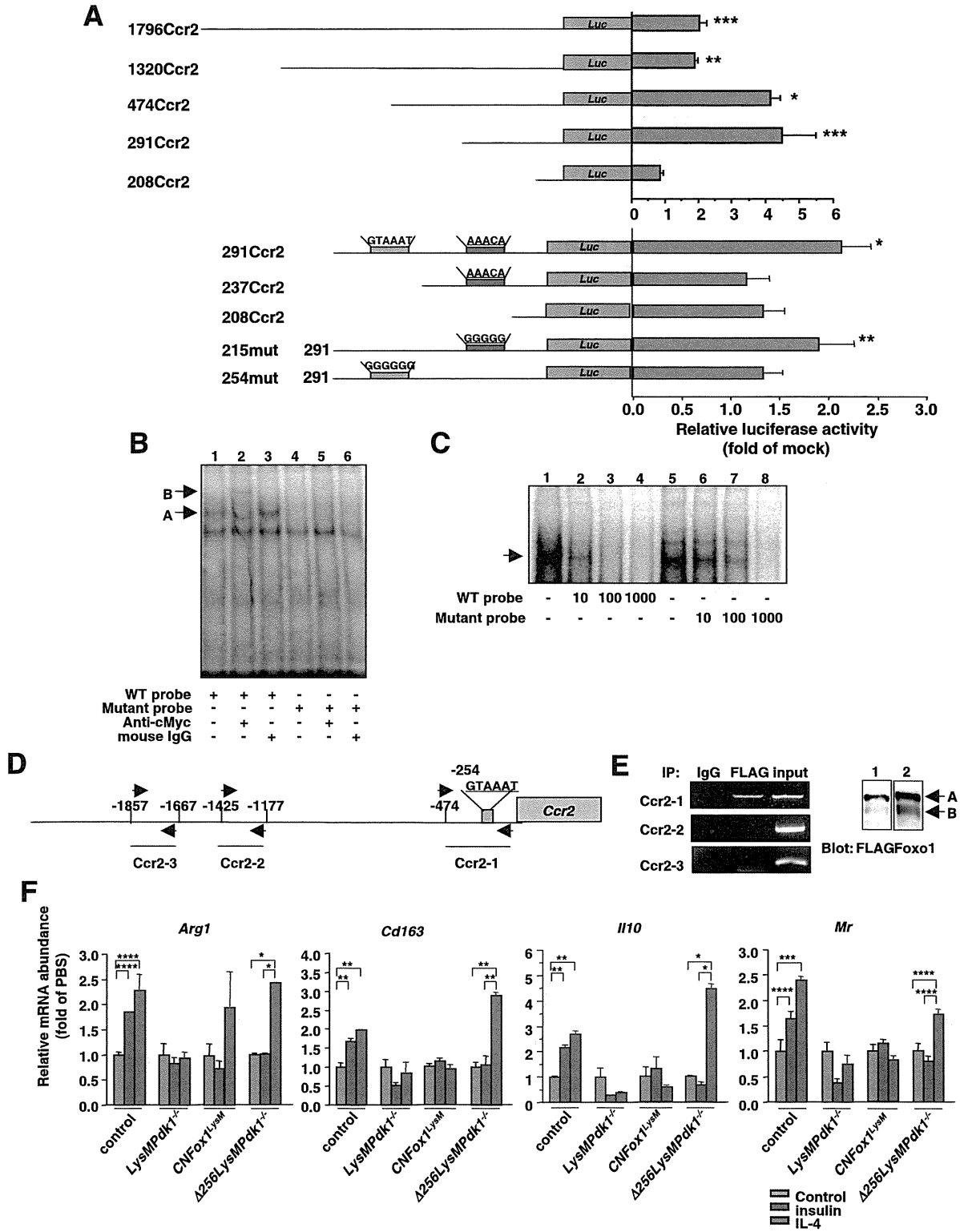

FIG. 6. *Ccr2* as a target gene of Foxo1 and the effects of insulin or IL-4 on genes for M2 signature. *A*: Effect of Foxo1 on Ccr2 promoter activity. Data were obtained from 10 experiments and are represented as means ± SEM of fold change from mock vector-transfected activity. $^{*}P < 0.001$, $^{**}P < 0.005$, and $^{***}P < 0.05$ (one-factor ANOVA of cells transfected with pCMV5/cMyc and pCVM5/cMyc-CNFoxo1 vector). *B*: EMSA of Foxo1 binding to DNA. The DNA probe was derived from a 31–base pair DNA covering the consensus Foxo1 binding site (−267/−237 nt) of the mouse Ccr2 promoter (*lanes 1–3*). A mutant DNA with an altered Foxo1 binding motif was used as a control (*lanes 4–6*). The position of the slowed complex is indicated as A, and the supershifted complex is indicated as B. *C*: Oligonucleotide probes corresponding to the Foxo1 binding site of the *Ccr2* promoter were incubated with nuclear extracts in the absence or presence of increasing amounts of unlabeled wild-type (*lanes 1–4*) or mutant oligonucleotide (*lanes 5–8*). *D*: Mouse *Ccr2* promoter and primer pairs used in ChIP assay. The magenta box indicates a consensus Foxo1 binding site. *E*: ChIP assays of RAW264.7 cells transduced with an adenovirus encoding CNFoxo1 and harvested 36 h after transduction (*left*). The PCR primers amplified the mouse *Ccr2* promoter sequence as shown in Fig. 5*G*. PCR reactions with total input chromatin are shown as control.

sequence from −254 to −249 nt in the mouse *Ccr2* promoter was the functional FRE.

Association of Foxo1 with the *Ccr2* promoter. To examine the ability of this putative FRE to bind Foxo1, we conducted an EMSA. Foxo1 caused significant retardation of the FRE DNA (Fig. 6*B*, *lane 1*). Inclusion of the anti-cMyc antibody resulted in a supershifted DNA band (Fig. 6*B*, *lane 2*). The same EMSA was performed using a mutant DNA containing five base substitutions within the FRE motif as a control. Alterations in the consensus FRE motif abrogated its ability to bind Foxo1 (Fig. 6*B*, *lane 4*). Incubating nuclear extracts from cells expressing cMyc-tagged Foxo1 with a probe encoding the 31–base pair FRE DNA sequence yielded a slower complex that was competed out by excess cold probe (Fig. 6*C*, *lanes 1–4*) but not mutant probe (Fig. 6*C*, *lanes 5–8*).

We performed a ChIP assay to determine the association between Foxo1 and the *Ccr2* promoter in RAW264.7 cells. Because of low levels of Foxo1 expression in RAW264.7 cells, we transduced cells with adenovirus encoding CNFoxo1. Using primers flanking the FRE motif within the *Ccr2* promoter (Fig. 6*D*), we detected a sequence-specific DNA corresponding to the proximal region (−474/9 nt) of the *Ccr2* promoter in immunoprecipitates obtained with anti-FLAG antibody (Fig. 6*E*). We also performed PCR analysis using a pair of off-target primers flanking distal regions (−1857/−1667 and −1425/−1177 nt). No specific DNA was amplified in the immunoprecipitates using normal mouse IgG or anti-FLAG antibody (Fig. 6*E*). These data confirm that Foxo1 directly binds the *Ccr2* promoter and that *Ccr2* is a target gene of Foxo1.

The Pdk1-Foxo1 pathway plays a role in alternative macrophage activation. To determine whether the Pdk1-Foxo1 pathway was essential for alternative activation of macrophages, we analyzed macrophage signatures in insulin- or IL-4–stimulated BMDMs from control, *LysMPdk1*$^{-/-}$, *CNFoxo1*^{LysM}, and *Δ256LysMPdk1*$^{-/-}$ mice. The signature genes, including *Arg1*, *Cd163*, *Il10*, and *Mr*, were significantly induced by insulin or IL-4 in BMDMs from control mice (Fig. 6*F*). In contrast, Pdk1 deficiency or constitutive Foxo1 activation completely abolished insulin- or IL-4–stimulated induction of the genes necessary for alternative macrophage activation (Fig. 6*F*). It is interesting that the expression of transactivation-defective (Δ256) Foxo1 rescued IL-4–induced, but not insulin-induced, gene expression (Fig. 6*F*). These data indicate that the Pdk1-Foxo1 pathway was required for the activation of macrophages via the alternative pathway.

A transactivation-defective (Δ256) Foxo1 partially protected against diet-induced insulin resistance. To determine whether blocking Foxo1 transactivation by expressing Δ256Foxo1 in ATMs would alleviate insulin resistance, we compared glucose homeostasis and insulin sensitivity in wild-type and *Δ256Foxo1*^{LysM} mice fed an HFD for 24 weeks. We observed no differences in body weight, glucose tolerance, or insulin secretion between genotypes (Fig. 7*A–C*). Furthermore, the *Δ256Foxo1*^{LysM} mice showed a weak but significant improvement in insulin sensitivity compared with wild-type mice (Fig. 7*D* and *E*).

After a 24-week HFD, *Δ256Foxo1*^{LysM} and wild-type mice had similar proportions of F4/80$^+$, F4/80$^+$CD11c$^+$CD206$^-$, and F4/80$^+$CD11c$^-$CD206$^+$ cells in adipose tissues (Fig. 7*F*). Moreover, in epididymal fat, no differences were observed in the gene expression profiles of M1 macrophages, including *Ccr2*, *Il1b*, *Tnfa*, and *Il6*. However, there was a significant increase in *Arg1* expression in *Δ256Foxo1*^{LysM} compared with control mice (Fig. 7*G*). Taken together, these data show that overexpression of Δ256Foxo1 in macrophages did not prevent glucose intolerance, but it did partially alleviate insulin resistance.

DISCUSSION

In the current study, we demonstrate that Pdk1 in ATMs inhibits recruitment of M1 macrophages into adipose tissues, while Foxo1 antagonizes these processes. These findings suggest that the Pdk1-Foxo1 signaling pathway in ATMs is important for regulation of chronic inflammation and insulin sensitivity in vivo (Fig. 8).

The key finding of the current study was that Foxo1 targeted *Ccr2* expression in macrophages. Ccr2 is the primary receptor for Mcp1/Ccl2, a member of the chemokine family of proteins. Ccr2 is expressed on circulating monocytes and ATMs, where it serves as a crucial monocyte recruitment factor by directing macrophages to sites of injury and inflammation. Furthermore, Ccr2 is important in the regulation of insulin sensitivity in vivo. Obesity increases the production of Ccl2 in adipose tissues, which leads to an accumulation of Ccl2-bound macrophages. When recruited macrophages are classically activated, they secrete proinflammatory cytokines, which leads to insulin resistance in various insulin-responsive tissues (2). Indeed, *Ccr2* deletion ameliorated insulin resistance in HFD-induced insulin resistance (37). Therefore, our observation of increased *Ccr2* expression in SVF M1 macrophages in *LysMPdk1*$^{-/-}$ and *CNFoxo1*^{LysM} mice was an important cue that insulin resistance had developed. Thus, the current study directly demonstrates that ATM Foxo1 played a pivotal role in regulating insulin sensitivity in vivo.

Nuclear accumulation of Foxo1 suddenly increased at 24 weeks of HFD, although phosphorylation of Pdk1 was not changed. These findings suggest that another signaling pathway may be involved in subcellular localization of Foxo1 in ATMs. One of the candidates is MST1, which mediates oxidative stress, phosphorylates FOXO proteins at a conserved site within the forkhead domain, disrupts their interaction with 14-3-3 proteins, and promotes FOXO nuclear translocation (27). Furthermore, JNK is known to phosphorylate and activate MST1 (30). HFD increased oxidative stress (18), leading to activation of JNK, MST1, and nuclear accumulation of Foxo1 (27). Of interest, we observed that H_2O_2 significantly increased at 24 weeks of HFD and that phosphorylation of MST1 also significantly increased at the same time. Therefore, oxidative stress in HFD may contribute to nuclear accumulation and activation of Foxo1. The findings suggest that nuclear accumulation of Foxo1 contributes to recruitment of M1 macrophages into adipose tissue during HFD.

Western blotting of transduced CNFoxo1 using anti-FLAG (*lane 1*) and anti-Foxo1 (*lane 2*) antibodies (*right*). The position of CNFoxo1 is indicated as A, and endogenous Foxo1 is indicated as B. *F*: Expression of genes *Arg1*, *Cd163*, *Il10*, and *Mr* of BMDM from the indicated genotypes. Cells were cultured for 2 days in the presence of PBS (control), insulin (100 nmol/L), or IL-4 (100 ng/mL). Values were normalized to β-actin expression and represent the means + SEM of fold of PBS in each genotype (8–10 mice per genotype). *$P < 0.001$, **$P < 0.005$, ***$P < 0.01$, and ****$P < 0.05$ (one-factor ANOVA among the indicated genotypes). WT, wild-type.

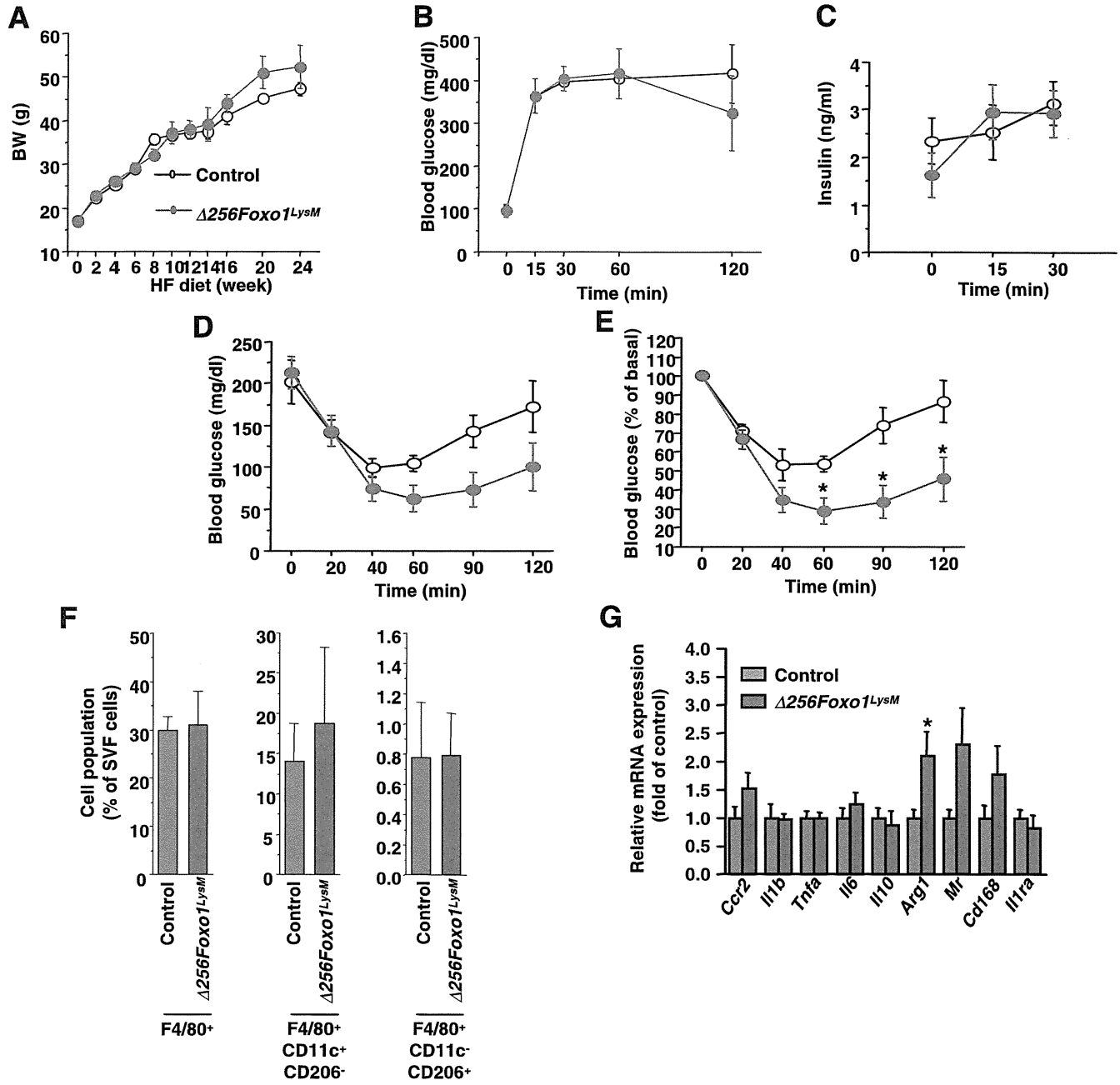

FIG. 7. A transactivation-defective (Δ256) Foxo1 partially protected against diet-induced insulin resistance. *A*: Body weight (BW) of control and *Δ256Foxo1*^{LysM} mice fed an HFD. Data are means + SEM of 20 mice in each genotype. *B*: IPGTT of control (open circle) and *Δ256Foxo1*^{LysM} (magenta circle) mice fed an HFD. Data are means + SEM of 20 mice in each genotype. *C*: Insulin secretion of control (open circle) and *Δ256Foxo1*^{LysM} (magenta circle) mice during IPGTT. Data are means + SEM of 20 mice in each genotype. *D* and *E*: ITT of control (open circle) and *Δ256Foxo1*^{LysM} (magenta circle) mice. Data are means + SEM of 20 mice in each genotype as absolute glucose values (*D*) and the percentages of basal values (*E*). *$P < 0.05$ (two-way repeated-measures ANOVA with an ad hoc multiple comparison method [Fisher's LSD test] of control vs. *Δ256Foxo1*^{LysM} mice). *F*: The percentages of F4/80$^+$, F4/80$^+$CD11c$^+$CD206$^-$, and F4/80$^+$CD11c$^-$CD206$^+$ cells within the viable SVF from 20- to 24-week-old mice of control and *Δ256Foxo1*^{LysM} mice. Data are means + SEM of 6 mice in each genotype analyzed in three independent experiments. *G*: Expression of genes in the epididymal fat of control and *Δ256Foxo1*^{LysM} mice. Values were normalized to β-actin expression and represent the means + SEM of 8–10 mice per genotype. *$P < 0.05$ (one-factor ANOVA of control vs. *Δ256Foxo1*^{LysM} mice).

However, we observed that expression of Δ256Foxo1 just partially protected against diet-induced insulin resistance and could not rescue *Ccr2* expression in mice fed an HFD for 24 weeks. Furthermore, the current study demonstrates that nuclear localization of Foxo1 started to occur at 24 weeks of HFD. Therefore, it is possible that nuclear localization of Foxo1 plays a role specifically in the late progression of diet-induced insulin resistance. From the current study, nuclear accumulation of Foxo1 in ATMs is only 40–45% of all F4/80$^+$ at 24 weeks of HFD, which means that an HFD cannot activate Foxo1 in ATMs completely. In contrast, the percentages of nuclear Foxo1 in ATMs of *LysMPdk1*$^{-/-}$ and *CNFoxo1*^{LysM} fed an HFD are ~70%. Therefore, the effect of loss of transactivation of Foxo1 on *Ccr2* expression in an

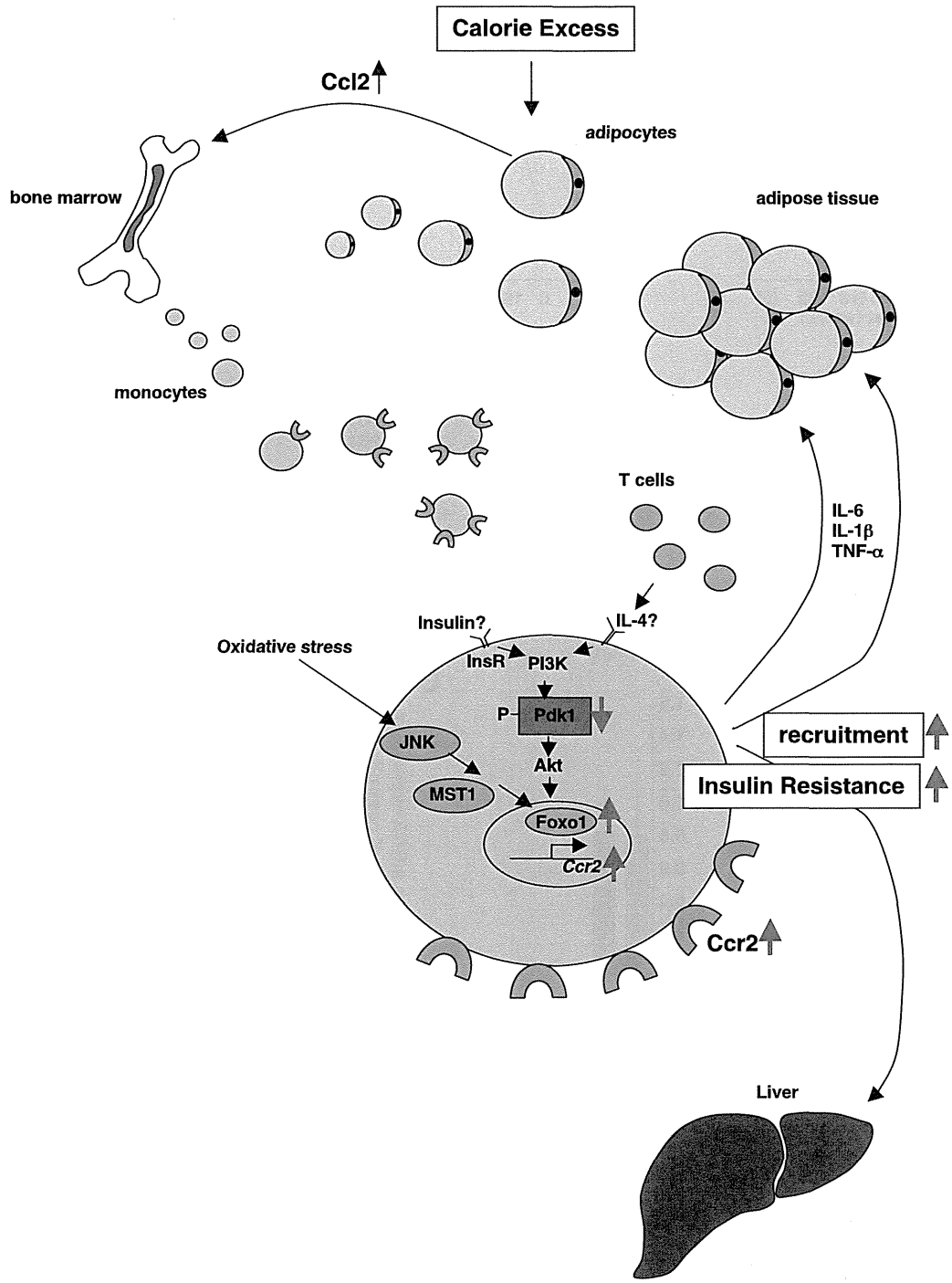

FIG. 8. Control of ATM function by Pdk1-Foxo1 pathway. Pdk1 is regulated by not only insulin but also cytokines, including IL-4, which is secreted from CD4$^+$ T cells or regulatory T cells. Furthermore, Foxo1 is regulated by not only Pdk1 but also oxidative stress through JNK and MST1. Phosphorylation of Pdk1 gradually declined during the HFD, but oxidative stress suddenly increased at the prolonged HFD, which is consistent with the time for the increased nuclear accumulation of Foxo1 in ATMs. Foxo1 directly regulates the expression of Ccr2, which upregulates the recruitment of macrophages in adipose tissue. PI3K, phosphatidylinositol 3-kinase.

HFD is small compared with *LysMPdk1*$^{-/-}$ mice. Alternatively, nuclear Foxo1 in myeloid cells may promote insulin resistance by other mechanisms than its role in the control of *Ccr2* gene expression. Furthermore, the *CNFoxo1*^{LysM} mice fed an NCD did not exhibit insulin resistance, while *LysMPdk1*$^{-/-}$ mice exhibited insulin resistance. These findings suggest that Foxo1 per se is not sufficient to cause HFD-induced insulin resistance, although Foxo1 may enhance the negative effect of an HFD on insulin sensitivity.

Our results provide direct evidence for the notion that ATM cell autonomous Pdk1-Foxo1 signaling regulates adipose tissue inflammation and insulin sensitivity in vivo. This finding may suggest a new target for pharmacological

intervention that could lead to novel therapeutic strategies for treating insulin resistance and type 2 diabetes.

ACKNOWLEDGMENTS

This work was supported by a grant from Nippon Boehringer Ingelheim Co., Ltd. to H.I. and a grant from Keio University Grant-in-Aid for Encouragement of Young Medical Scientists to Y.K. No other potential conflicts of interest relevant to this article were reported.

Y.K. researched data. J.N. conceived the hypothesis, designed and researched data, supervised the analyses, and wrote the manuscript. N.W., S.F., K.I., R.S., Y.H., and K.T. researched data. M.K. and T.N. generated and provided tissue-specific *Pdk1* knockout mice. A.Y. provided *LysMCre* mice and helpful discussion regarding experiments. M.O. researched data and assisted with data interpretation. H.I. supervised all experiments and assisted with preparation of the manuscript. J.N. is the guarantor of this work and, as such, had full access to all the data in the study and takes responsibility for the integrity of the data and the accuracy of the data analysis.

The authors thank Takahito Kaji (Training Department, Customer & Commercial Excellence, MSD K.K.) for analysis of data by two-way repeated-measures ANOVA.

REFERENCES

1. Qatanani M, Lazar MA. Mechanisms of obesity-associated insulin resistance: many choices on the menu. Genes Dev 2007;21:1443–1455
2. Olefsky JM, Glass CK. Macrophages, inflammation, and insulin resistance. Annu Rev Physiol 2010;72:219–246
3. Saltiel AR, Kahn CR. Insulin signalling and the regulation of glucose and lipid metabolism. Nature 2001;414:799–806
4. Welham MJ, Bone H, Levings M, et al. Insulin receptor substrate-2 is the major 170-kDa protein phosphorylated on tyrosine in response to cytokines in murine lymphohemopoietic cells. J Biol Chem 1997;272:1377–1381
5. Frittitta L, Grasso G, Munguira ME, Vigneri R, Trischitta V. Insulin receptor tyrosine kinase activity is reduced in monocytes from non-obese normoglycaemic insulin-resistant subjects. Diabetologia 1993;36:1163–1167
6. Zoppini G, Galante P, Zardini M, Muggeo M. Phosphotyrosine protein profiles in monocytes after insulin and IGF-1 stimulation. Eur J Clin Invest 1994;24:275–278
7. Liang CP, Han S, Okamoto H, et al. Increased CD36 protein as a response to defective insulin signaling in macrophages. J Clin Invest 2004;113:764–773
8. Han S, Liang CP, DeVries-Seimon T, et al. Macrophage insulin receptor deficiency increases ER stress-induced apoptosis and necrotic core formation in advanced atherosclerotic lesions. Cell Metab 2006;3:257–266
9. Senokuchi T, Liang CP, Seimon TA, et al. Forkhead transcription factors (FoxOs) promote apoptosis of insulin-resistant macrophages during cholesterol-induced endoplasmic reticulum stress. Diabetes 2008;57:2967–2976
10. Hashimoto N, Kido Y, Uchida T, et al. Ablation of PDK1 in pancreatic beta cells induces diabetes as a result of loss of beta cell mass. Nat Genet 2006;38:589–593
11. Iskandar K, Cao Y, Hayashi Y, et al. PDK-1/FoxO1 pathway in POMC neurons regulates Pomc expression and food intake. Am J Physiol Endocrinol Metab 2010;298:E787–E798
12. Su D, Coudriet GM, Hyun Kim D, et al. FoxO1 links insulin resistance to proinflammatory cytokine IL-1beta production in macrophages. Diabetes 2009;58:2624–2633
13. Fan W, Morinaga H, Kim JJ, et al. FoxO1 regulates Tlr4 inflammatory pathway signalling in macrophages. EMBO J 2010;29:4223–4236
14. Clausen BE, Burkhardt C, Reith W, Renkawitz R, Förster I. Conditional gene targeting in macrophages and granulocytes using LysMcre mice. Transgenic Res 1999;8:265–277
15. Nakae J, Cao Y, Oki M, et al. Forkhead transcription factor FoxO1 in adipose tissue regulates energy storage and expenditure. Diabetes 2008;57:563–576
16. Fujisaka S, Usui I, Bukhari A, et al. Regulatory mechanisms for adipose tissue M1 and M2 macrophages in diet-induced obese mice. Diabetes 2009;58:2574–2582
17. Nakae J, Biggs WH 3rd, Kitamura T, et al. Regulation of insulin action and pancreatic beta-cell function by mutated alleles of the gene encoding forkhead transcription factor Foxo1. Nat Genet 2002;32:245–253
18. Furukawa S, Fujita T, Shimabukuro M, et al. Increased oxidative stress in obesity and its impact on metabolic syndrome. J Clin Invest 2004;114:1752–1761
19. Odegaard JI, Ricardo-Gonzalez RR, Goforth MH, et al. Macrophage-specific PPARgamma controls alternative activation and improves insulin resistance. Nature 2007;447:1116–1120
20. Mauer J, Chaurasia B, Plum L, et al. Myeloid cell-restricted insulin receptor deficiency protects against obesity-induced inflammation and systemic insulin resistance. PLoS Genet 2010;6:e1000938
21. Nakae J, Kitamura T, Silver DL, Accili D. The forkhead transcription factor Foxo1 (Fkhr) confers insulin sensitivity onto glucose-6-phosphatase expression. J Clin Invest 2001;108:1359–1367
22. Nakae J, Cao Y, Daitoku H, et al. The LXXLL motif of murine forkhead transcription factor FoxO1 mediates Sirt1-dependent transcriptional activity. J Clin Invest 2006;116:2473–2483
23. Kubota N, Kubota T, Itoh S, et al. Dynamic functional relay between insulin receptor substrate 1 and 2 in hepatic insulin signaling during fasting and feeding. Cell Metab 2008;8:49–64
24. Nakae J, Kitamura T, Kitamura Y, Biggs WH 3rd, Arden KC, Accili D. The forkhead transcription factor Foxo1 regulates adipocyte differentiation. Dev Cell 2003;4:119–129
25. Casamayor A, Morrice NA, Alessi DR. Phosphorylation of Ser-241 is essential for the activity of 3-phosphoinositide-dependent protein kinase-1: identification of five sites of phosphorylation in vivo. Biochem J 1999;342:287–292
26. Accili D, Arden KC. FoxOs at the crossroads of cellular metabolism, differentiation, and transformation. Cell 2004;117:421–426
27. Lehtinen MK, Yuan Z, Boag PR, et al. A conserved MST-FOXO signaling pathway mediates oxidative-stress responses and extends life span. Cell 2006;125:987–1001
28. Choi J, Oh S, Lee D, et al. Mst1-FoxO signaling protects naïve T lymphocytes from cellular oxidative stress in mice. PLoS ONE 2009;4:e8011
29. Yuan Z, Lehtinen MK, Merlo P, Villén J, Gygi S, Bonni A. Regulation of neuronal cell death by MST1-FOXO1 signaling. J Biol Chem 2009;284:11285–11292
30. Bi W, Xiao L, Jia Y, et al. c-Jun N-terminal kinase enhances MST1-mediated pro-apoptotic signaling through phosphorylation at Serine 82. J Biol Chem 2010;285:6259–6264
31. Nakae J, Barr V, Accili D. Differential regulation of gene expression by insulin and IGF-1 receptors correlates with phosphorylation of a single amino acid residue in the forkhead transcription factor FKHR. EMBO J 2000;19:989–996
32. Murano I, Barbatelli G, Parisani V, et al. Dead adipocytes, detected as crown-like structures, are prevalent in visceral fat depots of genetically obese mice. J Lipid Res 2008;49:1562–1568
33. Sauter NS, Schulthess FT, Galasso R, Castellani LW, Maedler K. The anti-inflammatory cytokine interleukin-1 receptor antagonist protects from high-fat diet-induced hyperglycemia. Endocrinology 2008;149:2208–2218
34. Naito M. Macrophage differentiation and function in health and disease. Pathol Int 2008;58:143–155
35. Hanisch UK, Kettenmann H. Microglia: active sensor and versatile effector cells in the normal and pathologic brain. Nat Neurosci 2007;10:1387–1394
36. Weisberg SP, McCann D, Desai M, Rosenbaum M, Leibel RL, Ferrante AW Jr. Obesity is associated with macrophage accumulation in adipose tissue. J Clin Invest 2003;112:1796–1808
37. Weisberg SP, Hunter D, Huber R, et al. CCR2 modulates inflammatory and metabolic effects of high-fat feeding. J Clin Invest 2006;116:115–124

OPEN ACCESS Freely available online

PLOS ONE

Bile Acid Binding Resin Improves Metabolic Control through the Induction of Energy Expenditure

Mitsuhiro Watanabe[1,6]*, Kohkichi Morimoto[1], Sander M. Houten[2], Nao Kaneko-Iwasaki[1], Taichi Sugizaki[1], Yasushi Horai[1], Chikage Mataki[3], Hiroyuki Sato[4], Karin Murahashi[1], Eri Arita[1], Kristina Schoonjans[3], Tatsuya Suzuki[5], Hiroshi Itoh[1], Johan Auwerx[3]*

1 Department of Internal Medicine, School of Medicine, Keio University, Tokyo, Japan, **2** Laboratory Genetic Metabolic Diseases, Academic Medical Center, Amsterdam, The Netherlands, **3** Ecole Polytechnique Fédérale de Lausanne, Lausanne, Switzerland, **4** Department of Bioscience, Ehime University Graduate School of Medicine, Ehime, Japan, **5** Nippon Medical School, Tokyo, Japan, **6** Graduate School of Media and Governance, Keio University, Fujisawa-shi, Kanagawa, Japan

Abstract

Background: Besides well-established roles of bile acids (BA) in dietary lipid absorption and cholesterol homeostasis, it has recently become clear that BA is also a biological signaling molecule. We have shown that strategies aimed at activating TGR5 by increasing the BA pool size with BA administration may constitute a significant therapeutic advance to combat the metabolic syndrome and suggest that such strategies are worth testing in a clinical setting. Bile acid binding resin (BABR) is known not only to reduce serum cholesterol levels but also to improve glucose tolerance and insulin resistance in animal models and humans. However, the mechanisms by which BABR affects glucose homeostasis have not been established. We investigated how BABR affects glycemic control in diet-induced obesity models.

Methods and Findings: We evaluated the metabolic effect of BABR by administrating colestimide to animal models for the metabolic syndrome. Administration of BABR increased energy expenditure, translating into significant weight reduction and insulin sensitization. The metabolic effects of BABR coincide with activation of cholesterol and BA synthesis in liver and thermogenesis in brown adipose tissue. Interestingly, these effects of BABR occur despite normal food intake and triglyceride absorption. Administration of BABR and BA had similar effects on BA composition and thermogenesis, suggesting that they both are mediated *via* TGR5 activation.

Conclusion: Our data hence suggest that BABR could be useful for the management of the impaired glucose tolerance of the metabolic syndrome, since they not only lower cholesterol levels, but also reduce obesity and improve insulin resistance.

Citation: Watanabe M, Morimoto K, Houten SM, Kaneko-Iwasaki N, Sugizaki T, et al. (2012) Bile Acid Binding Resin Improves Metabolic Control through the Induction of Energy Expenditure. PLoS ONE 7(8): e38286. doi:10.1371/journal.pone.0038286

Editor: Massimo Federici, University of Tor Vergata, Italy

Received August 19, 2011; **Accepted** May 3, 2012; **Published** August 29, 2012

Funding: Funding was provided by grants of the Ecole Polytechnique Fédérale de Lausanne, the Swiss National Science Foundation, NIH, the Uehara Memorial Foundation, Takeda science foundation, the Sumitomo Foundation, Ono Medical Foundation, Astellas Foundation for Research on Metabolic Disorders, the Novartis Foundation (Japan) for Promotion of Science, the Japan Health Foundation, Kowa life science foundation and the Ministry of Education, Culture, Sports, Science and Technology of Japan for this study. The funders had no role in study design, data collection and analysis, decision to publish, or preparation of the manuscript.

Competing Interests: The authors have declared that no competing interests exist.

* E-mail: wmitsu@sc.itc.keio.ac.jp (MW); johan.auwerx@epfl.ch (JA)

Introduction

Bile acid (BA) is essential constituents of bile that facilitate dietary lipid absorption and cholesterol catabolism. BA also activates several signaling pathways, endowing them with an endocrine function. For instance, BA was shown to be natural ligands that activate the nuclear receptor farnesoid X receptor (FXR, NR1H4) [1–3], which controls both the synthesis and enterohepatic circulation of BA [4–5]. FXR induces the expression of the short heterodimer partner (SHP, NR0B2), an atypical nuclear receptor that acts as a corepressor. The FXR-mediated SHP induction contributes to the negative feedback regulation of BA biosynthesis, through inhibition of liver X receptor α and β (LXRα, NR1H3 and LXRβ, NR1H2) and liver receptor homolog-1 (LRH-1, NR5A2), both required for the transcription of the rate-limiting enzyme in the neutral BA biosynthesis pathway, cholesterol 7α-hydroxylase (CYP7A1) [6–11]. The FXR-mediated induction of FGF15/19 (FGF19 in human and its ortholog FGF15 in mouse) in intestinal epithelial cells also participates in the feedback repression of BA synthesis, via FGFR4 on hepatocytes [12–14]. Using a similar mechanism, the FXR-mediated SHP induction attenuates the capacity of LXR and LRH-1 to induce the expression of sterol regulatory element-binding protein (SREBP)-1c, the master regulator of lipogenesis, explaining the inhibition of hepatic fatty acid and triglyceride biosynthesis and VLDL production by BA administration [15]. Recently, it was reported that FXR deficiency improves glucose homeostasis in a mouse model for the metabolic syndrome [16]. In addition, we established that a synthetic FXR agonist (GW4064), deteriorates metabolic control in a diet-induced obesity mouse model [17]. These results suggest that the BA-specific nuclear

receptor FXR is involved in the pathogenesis of the metabolic syndrome.

BA may also signal in peripheral tissues through another pathway involving the binding and activation of TGR5, a G protein-coupled receptor (GPCR), leading to the induction of intracellular cyclic adenosine monophosphate (cAMP) levels [18–19]. The subsequent activation of type 2 iodothyronine deiodinase (D2), the enzyme which converts inactive thyroxine into active 3,5,3′-triiodothyronine [20] and hence determines thyroid hormone receptor saturation in cells, and of peroxisome proliferator-activated receptor (PPAR) γ coactivator-1α (PGC-1α), the master regulator of mitochondrial biogenesis [21], then stimulates energy expenditure in brown adipose tissue (BAT) (in rodents) and skeletal muscle (in humans) [22].Activation of this pathway explains how administration of BA to mouse models of obesity and diabetes induces weight loss and insulin sensitization. In addition, we reported that in mice, a synthetic FXR agonist (GW4064) reduced the BA pool and altered BA composition impairing peripheral energy metabolism possibly *via* TGR5 [17]. Furthermore, TGR5 activation enhances GLP-1 secretion from the enteroendocrine L-cell stimulating pancreatic insulin secretion [23]. Thus in addition to FXR, the BA-specific GPCR TGR5, is an attractive therapeutic target for treating metabolic syndrome.

These observations have built a strong case that BA has effects beyond the strict control of BA homeostasis and function as general metabolic integrators [24]. Bile acid binding resins (BABR), such as cholestyramine, is effective drugs for the treatment of coronary heart disease by lowering LDL-cholesterol as primary prevention, and for the treatment of cholestatic liver disease. BABR absorbs BA in the intestine thereby preventing their uptake in the ileum and interrupting their enterohepatic circulation. The resulting decrease of negative feedback signals will induce the expression of *Cyp7a1*. The subsequent decrease in intrahepatic cholesterol levels will on its turn activate SREBP-2, which induces the expression of the low density lipoprotein (LDL) receptor, to enhance cholesterol uptake, and of enzymes that synthesize cholesterol de novo, such as 3-hydroxy-3-methylglutaryl (HMG) CoA reductase. BABR was also reported to improve glycemic control in a type 2 diabetes mouse model [25], but the mechanism has not been established. We characterize here in detail the molecular and functional impact of a second generation BABR, colestimide [26], on metabolic homeostasis in animal models for the metabolic syndrome. Interestingly, colestimide not only reduces cholesterol levels but also decreases body weight and improves glucose tolerance, qualifying BABR as ideal agents to treat the metabolic syndrome. We suggest that a part of the anti-metabolic syndrome effect of BABR will be exerted by an alteration of the peripheral BA composition followed by TGR5 activation.

Materials and Methods

Materials

Cholic acid (CA) and cholestyramine were obtained from Sigma (St. Quentin Fallavier, France). Colestimide was a generous gift of Mitsubishi Pharmaceuticals.

Animal studies

All procedures undertaken in the present study conformed to the principles outlined in the *Guide for the Care and Use of Laboratory Animals* published by the USA National Institutes of Health (NIH Publication No. 85-23, revised 1996) and were approved by the Institutional Animal Care and Use Committee of Keio University School of Medicine (permission No. 08062-(2)). Male C57BL/6J mice, 6–7 weeks of age, were obtained from Charles River Laboratories France (l'Arbresle, France) and CLEA Japan Inc. (Tokyo, Japan), respectively. All mice were maintained in a temperature-controlled (23°C) facility with a 12 hours light/dark cycle and were given free access to food and water. The high-fat diet was obtained from Research diets (New Jersey, USA). The high-fat diet (D12492) contained 20 kcal% protein, 20 kcal% carbohydrate and 60 kcal% fat. For treatment with BA or BABR, mice were fed diets mixed with CA (0.5% w/w) or colestimide (2% w/w). Based on a daily food intake of 5 g, this resulted in a daily dose of colestimide 100 mg. The mice were fasted 4 hours before harvesting blood for subsequent blood measurements, and tissues for RNA isolation, lipid measurements and histology. Food intake was measured from the accumulated weight of the food for 1 week, with 5 mice in each group. Oxygen consumption was measured using the Oxymax apparatus (Columbus Instruments, Columbus, OH) [27].

Morphological studies

Pieces of mouse tissues were fixed in Bouin's solution, dehydrated in ethanol, embedded in paraffin, and cut at a thickness of 5 μm. Sections were deparaffinized, rehydrated, and stained with haematoxylin and eosin.

mRNA expression analysis by Q-RT-PCR

Expression levels were analyzed in cDNA synthesized from total mRNA using real-time PCR as described [22]. The sequences of the primer sets used are displayed in table 1.

Clinical biochemistry and evaluation of glucose and lipid homeostasis

An oral glucose tolerance test (OGTT) was performed in animals that were fasted overnight. Glucose was administered by gavage at a dose of 2 g/kg. An intra peritoneal insulin tolerance test (IPITT) was done in 4 h fasted animals. Insulin was injected at a dose of 0.75 U/kg. Glucose quantification was done with the Maxi Kit Glucometer 4 (Bayer Diagnostic, Puteaux, France) or Glucose RTU (bioMérieux Inc., Marcy l'Etoile, France). Plasma insulin concentrations were measured using ELISA for mouse (Cristal Chem Inc., Downers Grove, IL). HOMA-R was calculated by this formula: (fasting serum insulin concentration [μU/ml])*(fasting serum glucose concentration [mg/dl])/405. Free fatty acids, triglycerides, and total cholesterol were determined by enzymatic assays (Roche, Mannheim, Germany). LDL cholesterol was measured with plasma clinical chemistry analysis using AU-400 automated laboratory workstation and commercial reagents (Olympus France SA, Rungis, France) [28]. BA in enterohepatic organs were determined as described [29]. Lipid absorption was calculated as follows; (food lipid content – fecal lipid content)/food lipid content (×100(%)), with the food and feces consumed by/accumulated from 5 mice for 48 hours. To calculate the lipid absorption, TG was extracted from the accumulated feces by the classical Folch method [30] and measured as previously described [15].

Statistical analysis

Values were reported as mean +/− standard error (SEM). Statistical differences were determined using ANOVA (Statsview software, Abacus concepts, Inc., Berkeley, CA). Statistical significance is displayed as * ($P<0.05$) or ** ($P<0.01$) versus F.

Table 1. Primer sequences of genes used for quantification of mRNAs by real-time PCR.

Gene	Forward Primer (5′→3′)	Reverse Primer (5′→3′)
18s	GATGGGAAGTACAGCCAGGT	TTTCTTCAGCCTCTCCAGGT
Cyp7A1	TACAGAGTGCTGGCCAAGAG	TTCAAGGATGCACTGGAGAG
SHP	CAAGGAGTATGCGTACCTGAAG	GGCTCCAAGACTTCACACAGT
FXR	CAAAATGACTCAGGAGGAGTACG	GCCTCTCTGTCCTTGATGTATTG
PGC-1a	AAGGGCCAAACAGAGAGAGA	GCGTTGTGTCAGGTCTGATT
PEPCK	GGGAACTCACTACTCGGGAA	GCCAGGTATTTCTTCTTGCC
G6Pase	CCGGATCTACCTTGCTGCTCACTTT	TAGCAGGTAGAATCCAAGCGCGAAAC
SREBP-2	AAGTGACCGAGAGTCCCTTG	ACGTTGAGACTGCTCCACAG
HMGCR	TCGAAGGACGAGGAAAGACT	CGTCAACCATAGCTTCCGTA
LDLR	AGGCTGTGGGCTCCATAGG	TGCGGTCCAGGGTCATCT
PPARa	GGTGAGGAGAGCTCTGGAAG	GAAGCTGGAGAGAGGGTGTC
ACC	ACCCACTCCACTGTTTGTGA	CCTTGGAATTCAGGAGAGGA
SCD1	CTCCTGCTGATGTGCTTCAT	AAGGTGCTAACGAACAGGCT
D2	TTCTGAGCCGCTCCAAGT	GGAGCATCTTCACCCAGTTT
UCP-1	GGCCCTTGTAAACAACAAAATAC	GGCAACAAGAGCTGACAGTAAAT
FGF15	GGCAAGATATACGGGCTGAT	GATGGTGCTTCATGGATCTG
mCPT-1	GCACTGCAGCTCGCACATTACAA	CTCAGACAGTACCTCCTTCAGGAAA
Cyp8B1	GGAAGCCAAGAAGTCGTTCA	GACGCAGACTCTCCTCCATC
Cyp27A1	TCTGGCTACCTGCACTTCCT	CTGGATCTCTGGGCTCTTTG

doi:10.1371/journal.pone.0038286.t001

Results

BABR prevents the onset of diet-induced obesity

To evaluate the metabolic effects of a BABR in models of diet-induced obesity (DIO), we fed C57BL/6J mice normal chow, HF diet, or HF diet supplemented with either colestimide (2% w/w) or cholic acid (CA, 0.5% w/w) for 96 days. HF fed animals gained more weight than chow-fed animals. The animals fed with CA supplemented HF diet gained weight at a rate comparable to chow-fed mice. Colestimide had an even more pronounced effect in curbing weight gain. Since food intake and lipid absorption were not affected by CA and colestimide, these effects on body weight are probably mediated by increased energy expenditure (Fig. 1A). At necropsy, the weight of liver, epididymal white adipose tissue (epWAT) and BAT of HF fed animals was all significantly increased (Fig. 1B). The BAT was paler, indicative of increased fat accumulation, and there was an expansion of WAT surrounding the BAT (not shown). Both colestimide and CA completely prevented HF-induced changes in liver and adipose mass and morphology. High fat diet-induced significantly increased serum total cholesterol (T-C), LDL-cholesterol (LDL-C), fasting glucose and insulin levels. Colestimide ameliorated serum triglyceride (TG), T-C, LDL-C, fasting glucose and insulin levels significantly. CA administration exerted significant reduction of fasting glucose and insulin levels, but induced serum LDL-C level as expected (Fig. 1C). During OGTT, both colestimide and CA significantly reduced blood glucose concentrations to normalize the glucose tolerance of the mice with diet-induced obesity. Insulin sensitivity of the mice was also improved by colestimide and CA, shown in the result of IPITT (Fig. 1D). In KK-A^y mice, both colestimide and cholestiramine improved metabolic status (Text S1) without suppressing their food intake (Fig. S1A). The BABR significantly reduced epWAT weight gain, and also significantly improved serum metabolic index including TG, FFA, fasting glucose, insulin levels, and HOMA-R. Colestimide administration significantly improved liver weight gain and serum T-C level, either (Fig. S1B–D). The BABR-received KK-A^y mice exhibited significantly lower blood glucose during the OGTT (Fig. S1E). In the IPITT, the BABR reduced blood glucose level, but the improvement rate described in iAUC was not affected by the BABR administration (Fig. S1E). These data show that BABR improves metabolic control in mouse models for the metabolic syndrome.

BABR increases energy expenditure

The significant weight loss, in the wake of an unaltered food intake, suggested that BABR could stimulate energy expenditure and as such improve metabolic homeostasis. We hence analyzed the morphology of key metabolic tissues and performed indirect calorimetry in the C57BL/6J mice used in the HF study (see Fig. 1). This furthermore enabled us to compare the effect of the BABR with those of BA, which we characterized previously in this model [15] [22]. Liver sections of HF fed animals showed more unstained inclusions, indicative of steatosis, which were absent when the HF diet was supplemented with colestimide or CA (not shown and [15]). The HF diet induced significant adipocyte hypertrophy in both epWAT, characterized by a larger adipocyte volume (Fig. 2A), and BAT, typified by larger lipid vacuoles within the cells. This adipocyte hypertrophy was not observed when the HF diet was supplemented with either colestimide or CA. Electron microscopic analysis of BAT also showed more lipid vacuoles in HF fed animals when compared with chow fed animals or animals receiving HF diet combined with colestimide or CA (Fig. 2A,B&C). Compared with the HF diet, colestimide and CA supplementation increased the number of lamellar cristae in the mitochondria (Fig. 2C). Indirect calorimetry, showed a higher CO_2 production and O_2 consumption in animals fed a HF diet with either colestimide or CA when compared to animals on a HF or a

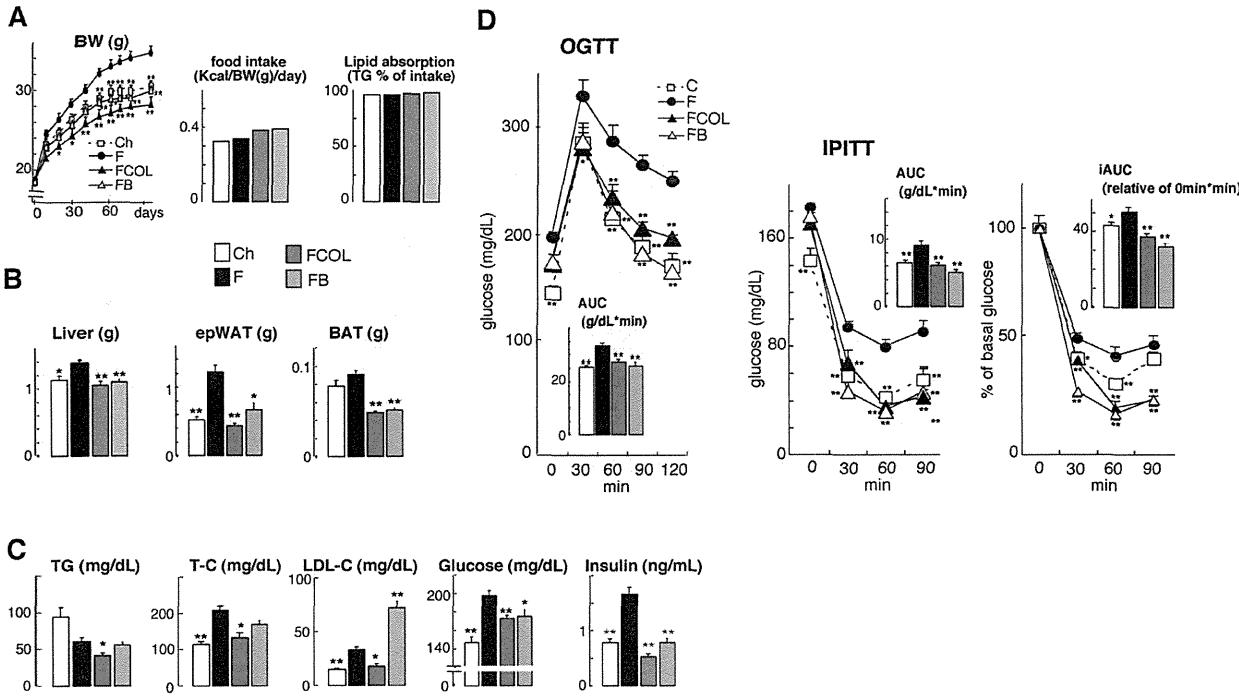

Figure 1. BA and BABR improve metabolic control in DIO C57BL/6J mice model. (A) Body weight, food intake and TG absorption (B) Liver, epididymal WAT (epWAT), and BAT weight change of C57BL/6J mice during 96 days on different diets. Ch stands for chow, F denotes HF diet, FCOL denotes HF diet+2.0% w/w colestimide and FB denotes HF diet+0.5% w/w CA. (C) Serum levels of TG, T-C, LDL-C, glucose and insulin in C57BL/6J mice on the indicated treatments. (D) Glucose levels during OGTT and IPITT in the different treatment groups (AUC is depicted in the inset). The OGTT were performed after an overnight fast after 9 weeks of administration. Glucose was administered by gavage at a dose of 2 g/kg. The IPITT were performed after 4 h fast after 10 weeks of administration. Insulin was injected at a dose of 0.75 U/kg. Data are expressed as the mean +/− SEM (n = 5–6). * ($P<0.05$) or ** ($P<0.01$) versus F.
doi:10.1371/journal.pone.0038286.g001

normal diet (Fig. 2D). We conclude from these experiments that feeding of colestimide or CA changes fat and energy metabolism most likely due to an effect on basal metabolic rate.

Molecular mechanism of BABR action

To identify the molecular drivers of the effects of BABR, we performed analysis of gene expression using Q-RT-PCR in liver, BAT, muscle and ileum of the C57BL/6J HF study (Fig. 1). Hepatic gene expression reflected the interruption of the enterohepatic cycle of BA by BABR and its consequences on BA production and cholesterol homeostasis. These changes were typified by the significant induction of *Cyp7a1* expression, subsequent to the reduction in *Shp*. *Cyp8b1* expression was significantly suppressed by CA administration, but was not affected by BABR administration. Gene expression of *Cyp27a1*, another rate-limiting enzyme participating in the alternative acidic BA synthesis pathway, was not affected by CA or BABR administration. The cholesterol depletion caused by colestimide stimulated BA production by CYP7A1, and then induced significantly increased expression levels of *Srebp-2* and its target genes including HMG-CoA reductase and LDL receptor. Genes involved in gluconeogenesis, such as phosphoenolpyruvate carboxykinase (*Pepck*) and glucose-6-phophatase (*G6Pase*) were affected. *Pepck* gene expression was significantly induced, and *G6Pase* gene expression was also stimulated as a consequence of the significant rise in the *Pgc-1a* expression, which stimulates gluconeogenesis. In contrast to colestimide, and as previously reported, the FXR agonist CA significantly induced *Shp* mRNA levels, which attenuates the expression of *Cyp7a1* and of the genes involved in cholesterol homeostasis. Genes involved in fatty acid oxidation (*Pparα*) and lipogenesis (acetyl-CoA carboxylase 1 (*Acc1*) and stearoyl-CoA desaturase-1 (*Scd1*)) were not changed in response to colestimide and CA (Fig. 3A).

In BAT, the expression of *Pgc-1α* and *D2* were both induced by colestimide and CA. As a consequence the expression of uncoupling protein-1 (*Ucp-1*) was also increased after both BABR and BA administration (Fig. 3B). Colestimide and CA treatment did not lead to significant differences in the expression of the genes involved in energy homeostasis in muscle (Fig. 3C). In ileum, the expression of *Fgf15*, which is one of the target genes of FXR, was significantly decreased by colestimide and increased by CA (Fig. 3D). In combination, the gene expression studies confirm that BAT and liver are the primary target organs that contribute to the beneficial effects of BABR on energy, lipid and glucose homeostasis. Remarkably, the effect on energy homeostasis induced by BABR was very similar to those observed after administration of CA (Figs. 1, 2, 3, Fig. S1 and [22]), despite the fact that BABR and BA has opposite actions on hepatic gene expression. Precisely, BABR administration induces *Cyp7a1* expression, while BA supplementation reduces expression of this gene, which is secondary to the changes in the BA pool size and serum BA levels. CA increased the BA pool and serum BA levels, but unexpectedly colestimide induced only a minor and non significant decrease in these parameters (Table 2). More striking, the changes in the composition of the BA pool and serum BA was similar after BABR or CA administration [22]. Both treatments

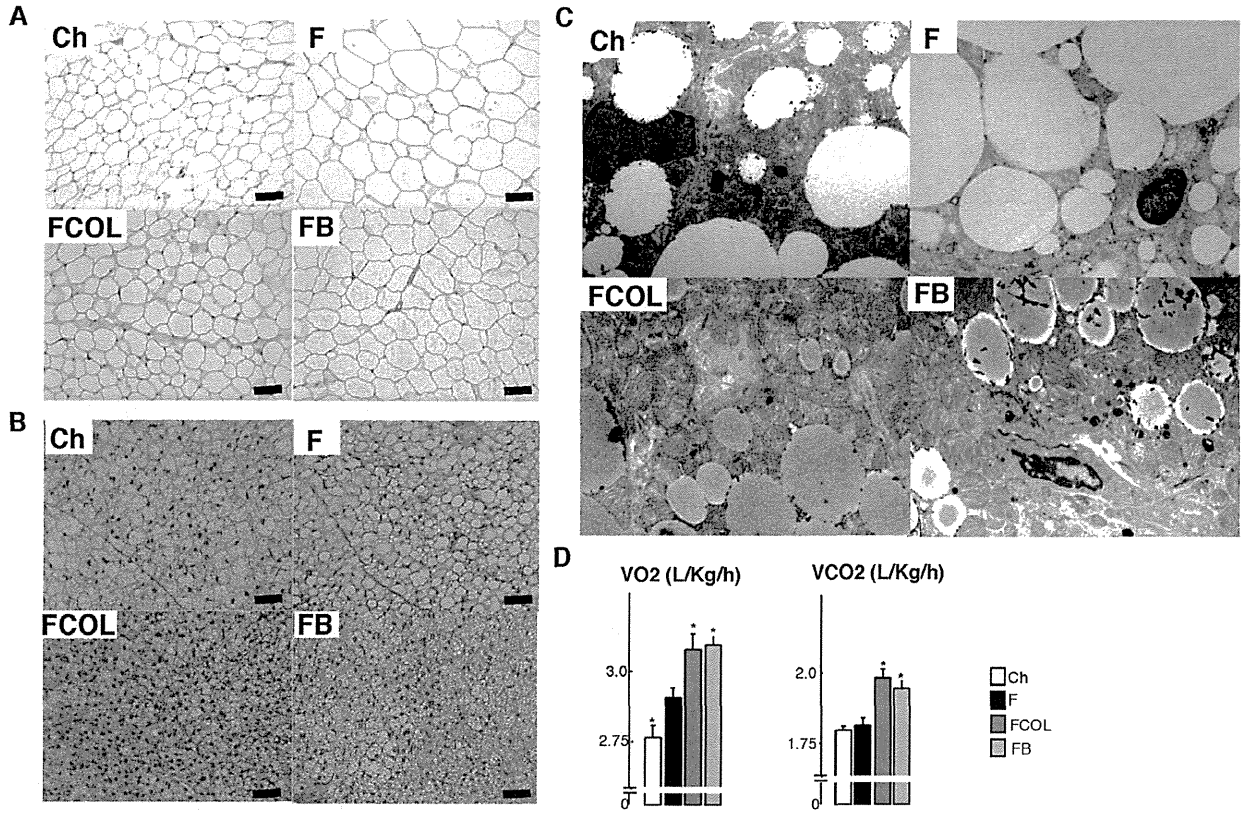

Figure 2. BABR increase energy expenditure. Hematoxylin and eosin (HE) stained epWAT (A) and BAT (B) sections of C57BL/6J animals treated with control or HF diet when indicated combined with colestimide or CA as specified in Fig. 1. Scale bar, 50 μm. (C) BAT analysis by transmission electron microscopy. (D) Averaged O_2 consumption (VO_2) and CO_2 production (VCO_2) as measured by indirect calorimetry in mice on the different diets as indicated. Data are expressed as the mean +/− SEM (n = 5–6). * ($P<0.05$) or ** ($P<0.01$) versus F.
doi:10.1371/journal.pone.0038286.g002

increased the relative contribution of CA and its derivatives, most notably tauroCA. Bile acids derived from chenodeoxyCA such as tauromuriCA were decreased by both BA supplementation and BABR treatment (Fig. 4 and [22]). BABR preferentially sequesters mono- and di-hydroxy BA and prevent them from enterohepatic recirculation hence inducing the de novo synthesis of CA.

Discussion

In the present study, we show that administration of BABR stimulated energy expenditure mediated by BAT, thereby preventing and reversing diet-induced obesity in mice. This phenomenon was accompanied by an improved glucose tolerance and insulin sensitization in a diet-induced obesity model (C57BL6/J (Fig. 1)). BABR also improved glucose tolerance in KK-A^y mice (Text S1 and Fig. S1). Brown adipose tissue is recently recognized as an important tissue of thermogenesis and energy homeostasis not only in rodents but also in man [31–33]. Our results indicate that therapy with colestimide, a new and better formulated BABR when compared with cholestyramine, could improve metabolic control also in humans suffering from the metabolic syndrome. In fact, colestimide decreased fasting glucose levels, but also reduced body weight, BMI, and visceral fat mass [34]. Furthermore, BABR was reported to improve obesity, insulin sensitivity and glycemic control in diabetes mellitus mouse model [25]. Furthermore, there is clinical evidence suggesting that BABR such as colesevelam may improve both lipid control and glycemic control in patients with type 2 diabetes that receive oral antihyperglycemic medications [35–37] [38,39]. Combined with the limited systemic toxicity ofBABR, which isnot absorbed, these compounds could constitute a significant advance in our therapeutic armamentarium to combat against metabolic syndrome. Although there is some evidence that the beneficial effects of BABR may be mediated through FXR, LXR, FGF15/19, and TGR5, but the exact molecular mechanisms are not yet clearly defined.

On a molecular and cellular level, BABR improves metabolic homeostasis through effects on liver and BAT (Fig. 5). The effects on liver are well known and include an induction of cholesterol and BA biosynthesis, subsequent to the fecal loss of bile acids caused by the BABR treatment. This underlies the cholesterol-lowering effect of BABR. The metabolic effects on BAT have not been reported before and phenocopy the changes seen after treatment of rodents with primary BA, such as CA [22]. This is surprising, since treatment with BABR and BA has opposite actions on most parameters of BA homeostasis. CA administration increases FXR activation, whereas BABR treatment decreases it. CA administration decreases the BA synthesis, whereas BABR treatment increases it. However, BABR and CA had similar effects on BA composition. Both treatments increased the relative contribution of CA and its derivatives, most notably deoxyCA, tauro-deoxyCA and tauroCA. Bile acids derived from chenodeox-

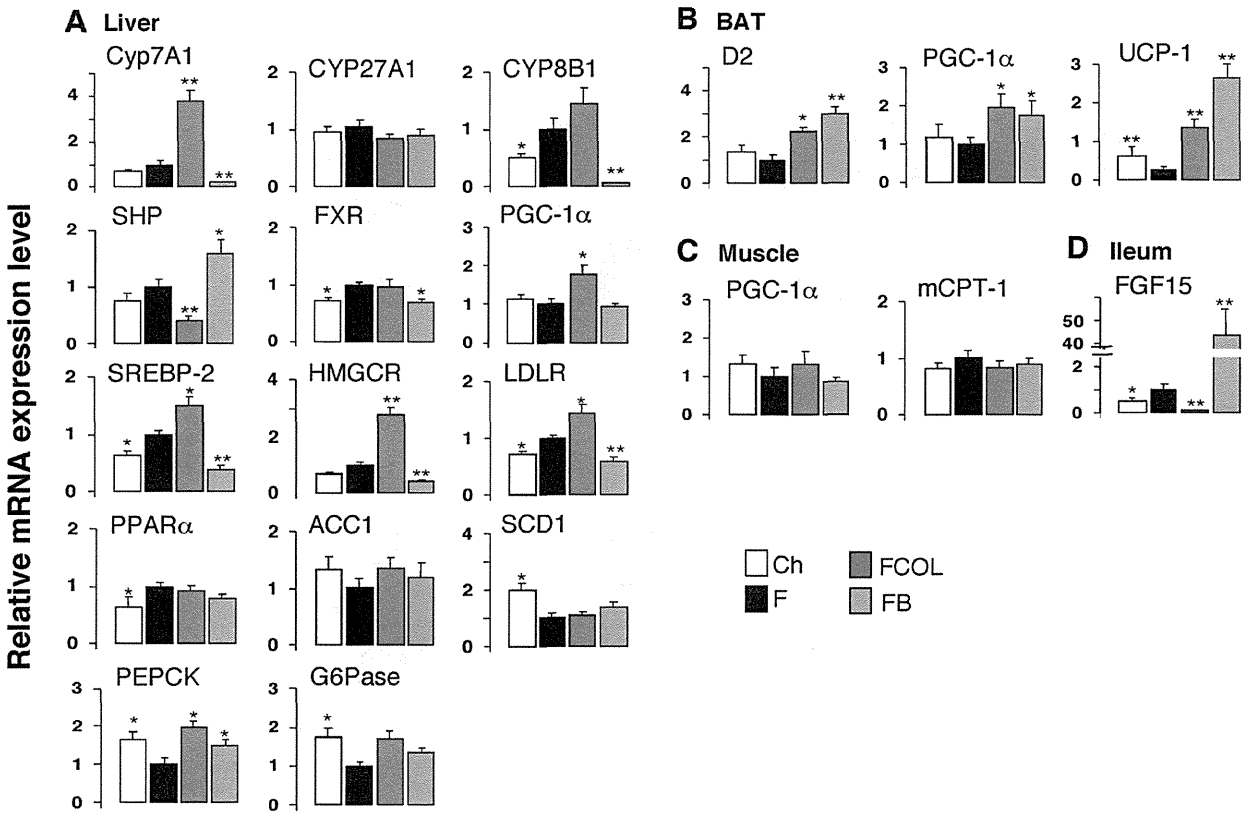

Figure 3. Gene expression in liver, BAT, muscle and ileum. (A) mRNA expression levels of *Cyp7a1*, *Cyp8b1*, *Cyp27a1*, *Shp*, *Fxr*, *Pgc-1α*, *Pepck*, *G6Pase*, *Srebp-2*, HMG-CoA reductase, LDL-Receptor, *Pparα*, *Acc1* and *Scd1* were determined using quantitative RT-PCR in liver of C57BL/6J mice treated as described in Fig. 1A. (B) mRNA expression levels of *D2*, *Pgc-1α* and *Ucp-1* in BAT. (C) *Pgc-1α* and *mCpt-1* in muscle. (D) *Fgf15* in ileum. Treatments and abbreviations are identical to those specified in Fig. 1A. Mice were fasted 4 hours before sacrifice and tissue collection. Data are expressed as the mean +/− SEM (n = 5–6). * ($P<0.05$) or ** ($P<0.01$) versus F.
doi:10.1371/journal.pone.0038286.g003

yCA such as muriCA and tauromuriCA were decreased. In addition to our studies in mice, colestimide treatment of hypercholesterolemia patients significantly increased CA in bile [40]. The most likely explanation for this specific increase in BA species derived from CA, is the fact that colestimide has a high adsorptive capacity for mono- and di-hydroxy BA like chenodeoxyCA and lithoCA, but a relative low capacity for the tri-hydroxy BA such as CA. In addition, the induced BA biosynthesis during colestimide treatment might produce more CA than chenodeoxyCA [41]. Increased BA pool size and plasma BA levels are fine indicator for TGR5 activation [22] [17]. This time, we focus on the importance of bile acid composition to improve metabolic status. TGR5 is activated by almost all BA including mono- and di-hydroxy BA. Some of the BA like ursodeoxyCA have little activity on TGR5, but no inhibitory BA was identified in our test of over 60 BA and BA derivatives for antagonistic effects on TGR5 (data not shown). Most importantly, BABR administration induced levels of tauroCA, a relatively potent TGR5 agonist [22], which could be the key to the anti-metabolic syndrome effect of BABR administration. In agreement with this, reduction of BA pool size and tauroCA levels by the administration of the synthetic FXR agonist GW4064, exacerbated the effects of HF feeding [17].

It is conceivable that BABR, such as colestimide and cholestyramine that are mainly active in the intestinal tract, could affect the production of incretins, such as FGF15, cholecystokinin (CCK) and glucagon like peptide-1 (GLP-1). FGF15 is interesting in this respect, since transgenic mice that overexpress the human *Fgf15* ortholog *Fgf19* in the muscle or in a more general pattern have increased metabolic rate and decreased adiposity [42]. BABR, however, decreases expression of *Fgf15* (Fig. 3D), whereas CA has the opposite effect, making it unlikely that it underlies the common metabolic effects of BABR. GLP-1 has glucose-dependent insulinotropic actions on the pancreatic beta-cells and has recently been associated with bile acids because its release was stimulated in an enteroendocrine cell line via TGR5, a GPCR specific for bile acids [23]. BABR may have an effect on the intestinal secretion of GLP-1, according to recent reports [43]. Indeed, we found that GLP-1 secretion was stimulated by BABR administration (unpublished data), which may contribute to the other beneficial effects of BABR. CCK is another good candidate, since cholestyramine can increase CCK production but also pancreatic beta cell function [44–45]. In addition CCK has been linked to increased sympathetic activity to BAT [46–47]. To date, effects of BABR on incretins and BAT have not been sufficiently studied.

Taken together, our data show that BABR activates energy expenditure, resulting in weight loss and improved glucose tolerance in animal models suffering from the metabolic syndrome, in a mechanism very similar to BA administration [22]. The alteration of BA composition, which occurs after BABR

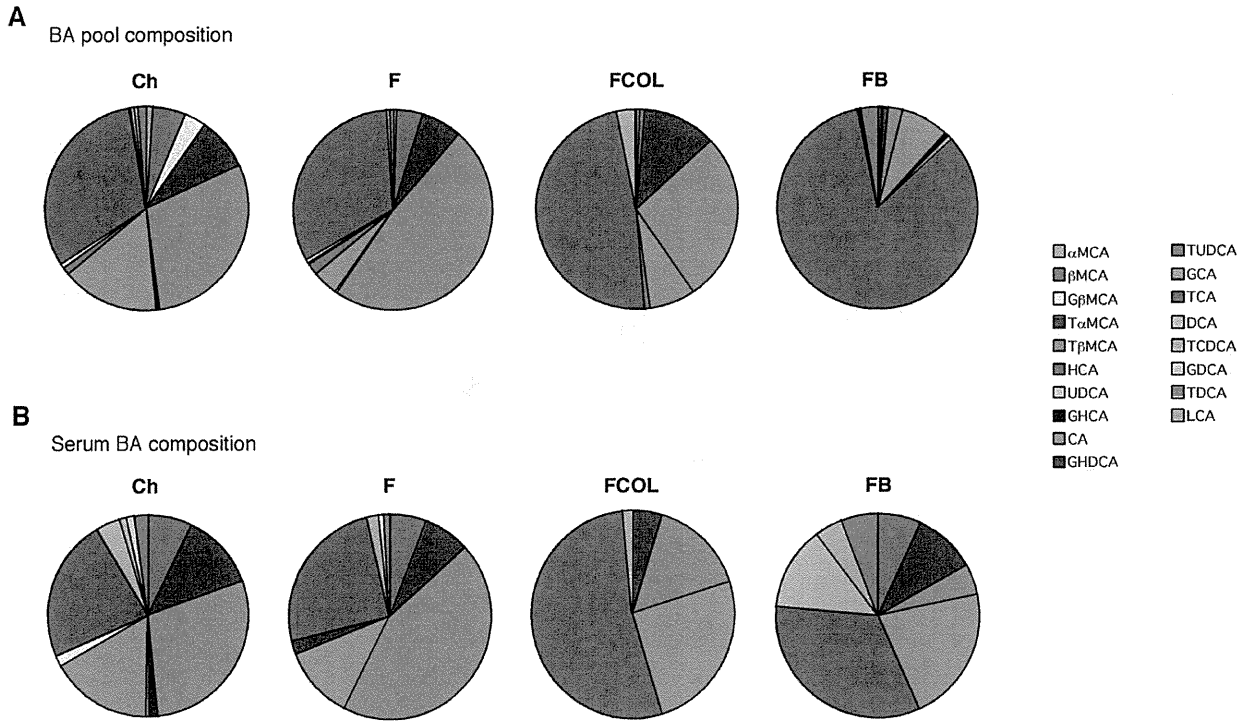

Figure 4. Bile acid composition in the enterohepatic organs and serum. Bile acid composition in the enterohepatic organs and serum of C57BL/6J fed with high fat diet (Fig. 1A) after treatment with colestimide or CA. Undefined abbreviations are: G, glycol; T, tauro; CD, chenodeoxy; D, deoxy; H, hyo; HD, hyodeoxy; UD, ursodeoxy; L, litho; M, muri.
doi:10.1371/journal.pone.0038286.g004

and CA administration, more specifically the increase of tauroCA, may be the key to improve the metabolic status. A recent study in man employing colesevalam treatment in type 2 diabetic patients revealed no correlation energy expenditure with plasma BA levels [48]. Another report showed that BA kinetics caused by BABR administration could not affect the improvement of glycemic control in patients with T2DM [49]. In fact, biophysiological roles and significances of the each composition of the BA profiles might not be identical in human and mice, and it is difficult to make a plain comparison between the report and our result. Futhermore, in the report, the 'BA kinetics' was just a cholic acid or total bile acid synthesis. More precise analysis according to BA profiles, as we performed in this article, would provide a clue to solve the mechanism of improved glycemic control by BABR. These reports illustrate that the mechanisms involved in the beneficial effects of BABR in humans are still controversial and further investigation is warranted. Our previous study demonstrated one of the various mechanisms of BABR in anti-metabolic syndrome effect. Our

Table 2. BA pool size and serum BA concentration in C57BL/6J mice.

	BA pool size (nmol/g Liver+Intestine)	Serum BA (μM)
Ch	9852.6+/−191.2[A]	15.23+/−2.23
F	9130.4+/−261.6	13.83+/−1.80
FCOL	8643.4+/−254.8	11.84+/−1.68
FB	22867.0+/−145.3[B]	18.21+/−1.16[A]

Ch denotes chow, F denotes HF diet, FCOL denotes HF diet+2% w/w colestimide and FB denotes HF diet+0.5% w/w CA as specified in Fig. 1A. Data are expressed as mean +/− SEM (n = 5–6).
[A]$P<0.05$ versus F.
[B]$P<0.01$ versus F.
doi:10.1371/journal.pone.0038286.t002

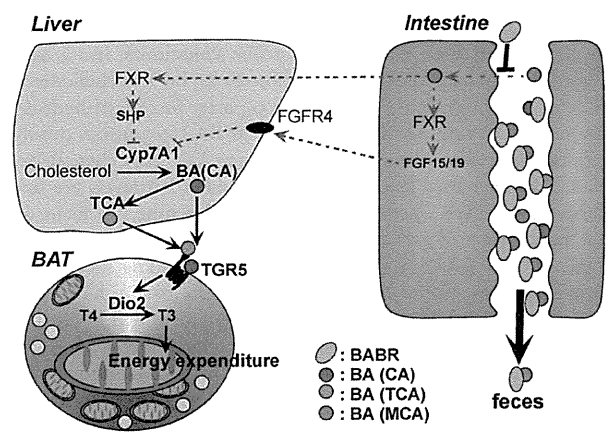

Figure 5. Changes in energy metabolism by BABR administration. Administration of BABR to animals leads to induction of bile acid synthesis and as a consequence a relative increase in CA and TCA. This translates into induced energy expenditure in brown adipose tissue, hence improving obesity and diabetes.
doi:10.1371/journal.pone.0038286.g005

findings in mice could be useful clues to elucidate the signaling functions of BA in man.

Supporting Information

Figure S1 BABR improves metabolic control in KK-A^y mice. (A) Body weight (BW) and food intake change of KK-A^y mice. Ch denotes chow, COL denotes chow+colestimide and CHO denotes chow+cholestyramine. (B) A comparison of the weight of liver, epididymal WAT (epWAT) and BAT fat pads after the different interventions. (C) Serum levels of triglycerides (TG), free fatty acids (FFA), total cholesterol (T-C) in KK-A^y mice on the indicated treatments. (D) Serum levels of glucose and insulin in KK-A^y mice on the indicated treatments. The HOMA-IR is calculated as described in the materials and methods. (E) Glucose levels during an OGTT and IPITT, and area under the curve (AUC) and integrated areas under the curve (iAUC) in KK-A^y mice in the different treatment groups. The OGTT were performed after an overnight fast after 2 weeks of administration. Glucose was administered by gavage at a dose of 1 g/kg. The IPITT were performed after 4 hours fast after 3 weeks of administration. Insulin was injected at a dose of 0.75 U/kg. Data are expressed as the mean +/− SEM (n = 5–6). # ($P<0.05$) or ## ($P<0.01$) versus Ch. Further description about the materials and methods of the experiments is included in "Materials and Methods S1".
(DOC)

Text S1
(DOCX)

Materials and Methods S1
(DOC)

Acknowledgments

The authors thank Pierre Chambon, Ron Evans, Kazuo Suzuki, Kanami Sugimoto-Kawabata, Kaoru Sakai and Satoshi Iwasaki for helpful discussions, and Tomomi Taniguchi, Nadia Messaddeq, Henk Overmars and Marie-France Champy for technical assistance. In memory of Shinya Inoue, who made a great contribution to this study during his short life.

Author Contributions

Conceived and designed the experiments: MW SMH JA. Performed the experiments: MW KM CM T. Sugizaki EA HS YH NKI K. Murahashi. Analyzed the data: MW K. Morimoto. Contributed reagents/materials/analysis tools: T. Sugizaki YH T. Suzuki KS. Wrote the paper: MW K. Morimoto SMH HI JA.

References

1. Makishima M, Okamoto AY, Repa JJ, Tu H, Learned RM, et al. (1999) Identification of a nuclear receptor for bile acids. Science 284: 1362–1365.
2. Parks DJ, Blanchard SG, Bledsoe RK, Chandra G, Consler TG, et al. (1999) Bile acids: natural ligands for an orphan nuclear receptor. Science 284: 1365–1368.
3. Wang H, Chen J, Hollister K, Sowers LC, Forman BM (1999) Endogenous bile acids are ligands for the nuclear receptor FXR/BAR. Mol Cell 3: 543–553.
4. Houten SM, Auwerx J (2004) The enterohepatic nuclear receptors are major regulators of the enterohepatic circulation of bile salts. Ann Med 36: 482–491.
5. Russell DW (2003) The enzymes, regulation, and genetics of bile acid synthesis. Annu Rev Biochem 72: 137–174.
6. Brendel C, Schoonjans K, Botrugno OA, Treuter E, Auwerx J (2002) The small heterodimer partner interacts with the liver X receptor alpha and represses its transcriptional activity. Mol Endocrinol 16: 2065–2076.
7. Goodwin B, Jones SA, Price RR, Watson MA, McKee DD, et al. (2000) A regulatory cascade of the nuclear receptors FXR, SHP-1, and LRH-1 represses bile acid biosynthesis. Mol Cell 6: 517–526.
8. Kerr TA, Saeki S, Schneider M, Schaefer K, Berdy S, et al. (2002) Loss of nuclear receptor SHP impairs but does not eliminate negative feedback regulation of bile acid synthesis. Dev Cell 2: 713–720.
9. Lu TT, Makishima M, Repa JJ, Schoonjans K, Kerr TA, et al. (2000) Molecular basis for feedback regulation of bile acid synthesis by nuclear receptors. Mol Cell 6: 507–515.
10. Sinal CJ, Tohkin M, Miyata M, Ward JM, Lambert G, et al. (2000) Targeted disruption of the nuclear receptor FXR/BAR impairs bile acid and lipid homeostasis. Cell 102: 731–744.
11. Wang L, Lee YK, Bundman D, Han Y, Thevananther S, et al. (2002) Redundant pathways for negative feedback regulation of bile acid production. Dev Cell 2: 721–731.
12. Holt JA, Luo G, Billin AN, Bisi J, McNeill YY, et al. (2003) Definition of a novel growth factor-dependent signal cascade for the suppression of bile acid biosynthesis. Genes Dev 17: 1581–1591.
13. Inagaki T, Choi M, Moschetta A, Peng L, Cummins CL, et al. (2005) Fibroblast growth factor 15 functions as an enterohepatic signal to regulate bile acid homeostasis. Cell Metab 2: 217–225.
14. Stroeve JH, Brufau G, Stellaard F, Gonzalez FJ, Staels B, et al. (2010) Intestinal FXR-mediated FGF15 production contributes to diurnal control of hepatic bile acid synthesis in mice. Lab Invest 90: 1457–1467.
15. Watanabe M, Houten SM, Wang L, Moschetta A, Mangelsdorf DJ, et al. (2004) Bile acids lower triglyceride levels via a pathway involving FXR, SHP, and SREBP-1c. J Clin Invest 113: 1408–1418.
16. Prawitt J, Abdelkarim M, Stroeve JH, Popescu I, Duez H, et al. (2011) Farnesoid x receptor deficiency improves glucose homeostasis in mouse models of obesity. Diabetes 60: 1861–1871.
17. Watanabe M, Horai Y, Houten SM, Morimoto K, Sugizaki T, et al. (2011) Lowering bile acid pool size with a synthetic FXR agonist induces obesity and diabetes through reduced energy expenditure. J Biol Chem.
18. Kawamata Y, Fujii R, Hosoya M, Harada M, Yoshida H, et al. (2003) A G protein-coupled receptor responsive to bile acids. J Biol Chem 278: 9435–9440.
19. Maruyama T, Miyamoto Y, Nakamura T, Tamai Y, Okada H, et al. (2002) Identification of membrane-type receptor for bile acids (M-BAR). Biochem Biophys Res Commun 298: 714–719.
20. Bianco AC, Salvatore D, Gereben B, Berry MJ, Larsen PR (2002) Biochemistry, cellular and molecular biology, and physiological roles of the iodothyronine selenodeiodinases. Endocr Rev 23: 38–89.
21. Puigserver P, Spiegelman BM (2003) Peroxisome proliferator-activated receptor-gamma coactivator 1 alpha (PGC-1 alpha): transcriptional coactivator and metabolic regulator. Endocr Rev 24: 78–90.
22. Watanabe M, Houten SM, Mataki C, Christoffolete MA, Kim BW, et al. (2006) Bile acids induce energy expenditure by promoting intracellular thyroid hormone activation. Nature 439: 484–489.
23. Thomas C, Gioiello A, Noriega L, Strehle A, Oury J, et al. (2009) TGR5-mediated bile acid sensing controls glucose homeostasis. Cell Metab 10: 167–177.
24. Houten SM, Watanabe M, Auwerx J (2006) Endocrine functions of bile acids. Embo J 25: 1419–1425.
25. Kobayashi M, Ikegami H, Fujisawa T, Nojima K, Kawabata Y, et al. (2007) Prevention and treatment of obesity, insulin resistance, and diabetes by bile acid-binding resin. Diabetes 56: 239–247.
26. Homma Y, Kobayashi T, Yamaguchi H, Ozawa H, Sakane H, et al. (1997) Specific reduction of plasma large, light low-density lipoprotein by a bile acid sequestering resin, cholebine (MCI-196) in type II hyperlipoproteinemia. Atherosclerosis 129: 241–248.
27. Picard F, Gehin M, Annicotte J, Rocchi S, Champy MF, et al. (2002) SRC-1 and TIF2 control energy balance between white and brown adipose tissues. Cell 111: 931–941.
28. Mataki C, Magnier BC, Houten SM, Annicotte JS, Argmann C, et al. (2007) Compromised intestinal lipid absorption in mice with a liver-specific deficiency of liver receptor homolog 1. Mol Cell Biol 27: 8330–8339.
29. Sakakura H, Suzuki M, Kimura N, Takeda H, Nagata S, et al. (1993) Simultaneous determination of bile acids in rat bile and serum by high-performance liquid chromatography. J Chromatogr 621: 123–131.
30. Folch J, Lees M, Sloane-Stanley GH (1957) A simple method for the isolation and purification of total lipids from animal tissues. J Biol Chem 226: 497–509.
31. van Marken Lichtenbelt WD, Vanhommerig JW, Smulders NM, Drossaerts JM, Kemerink GJ, et al. (2009) Cold-activated brown adipose tissue in healthy men. N Engl J Med 360: 1500–1508.
32. Cypess AM, Lehman S, Williams G, Tal I, Rodman D, et al. (2009) Identification and importance of brown adipose tissue in adult humans. N Engl J Med 360: 1509–1517.
33. Virtanen KA, Lidell ME, Orava J, Heglind M, Westergren R, et al. (2009) Functional brown adipose tissue in healthy adults. N Engl J Med 360: 1518–1525.
34. Suzuki T, Oba K, Igari Y, Watanabe K, Matsumura N, et al. (2012) Effects of bile-acid-binding resin (colestimide) on blood glucose and visceral fat in Japanese patients with type 2 diabetes mellitus and hypercholesterolemia: an open-label, randomized, case-control, crossover study. J Diabetes Complications 26: 34–39.

35. Garg A, Grundy SM (1994) Cholestyramine therapy for dyslipidemia in non-insulin-dependent diabetes mellitus. A short-term, double-blind, crossover trial. Ann Intern Med 121: 416–422.
36. Bays HE, Goldberg RB, Truitt KE, Jones MR (2008) Colesevelam hydrochloride therapy in patients with type 2 diabetes mellitus treated with metformin: glucose and lipid effects. Arch Intern Med 168: 1975–1983.
37. Fonseca VA, Rosenstock J, Wang AC, Truitt KE, Jones MR (2008) Colesevelam HCl improves glycemic control and reduces LDL cholesterol in patients with inadequately controlled type 2 diabetes on sulfonylurea-based therapy. Diabetes Care 31: 1479–1484.
38. Goldberg RB, Fonseca VA, Truitt KE, Jones MR (2008) Efficacy and safety of colesevelam in patients with type 2 diabetes mellitus and inadequate glycemic control receiving insulin-based therapy. Arch Intern Med 168: 1531–1540.
39. Zieve FJ, Kalin MF, Schwartz SL, Jones MR, Bailey WL (2007) Results of the glucose-lowering effect of WelChol study (GLOWS): a randomized, double-blind, placebo-controlled pilot study evaluating the effect of colesevelam hydrochloride on glycemic control in subjects with type 2 diabetes. Clin Ther 29: 74–83.
40. Kajiyama G, Tazuma S, Yamashita G, Ochi H, Miura H, et al. (1996) Effect of MCI-196 on biliary lipids metabolism in patients with hypercholesterolemia. J Clin Ther Med 12: 1349–1359.
41. Garbutt JT, Kenney TJ (1972) Effect of cholestyramine on bile acid metabolism in normal man. J Clin Invest 51: 2781–2789.
42. Tomlinson E, Fu L, John L, Hultgren B, Huang X, et al. (2002) Transgenic mice expressing human fibroblast growth factor-19 display increased metabolic rate and decreased adiposity. Endocrinology 143: 1741–1747.
43. Katsuma S, Hirasawa A, Tsujimoto G (2005) Bile acids promote glucagon-like peptide-1 secretion through TGR5 in a murine enteroendocrine cell line STC-1. Biochem Biophys Res Commun 329: 386–390.
44. Kogire M, Gomez G, Uchida T, Ishizuka J, Greeley GH, Jr., et al. (1992) Chronic effect of oral cholestyramine, a bile salt sequestrant, and exogenous cholecystokinin on insulin release in rats. Pancreas 7: 15–20.
45. Koop I, Fellgiebel A, Koop H, Schafmayer A, Arnold R (1988) Effect of cholestyramine on plasma cholecystokinin and pancreatic polypeptide levels, and exocrine pancreatic secretion. Eur J Clin Invest 18: 517–523.
46. Shido O, Yoneda Y, Nagasaka T (1989) Changes in brown adipose tissue metabolism following intraventricular vasoactive intestinal peptide and other gastrointestinal peptides in rats. Jpn J Physiol 39: 359–369.
47. Yoshimatsu H, Egawa M, Bray GA (1992) Effects of cholecystokinin on sympathetic activity to interscapular brown adipose tissue. Brain Res 597: 298–303.
48. Brufau G, Bahr MJ, Staels B, Claudel T, Ockenga J, et al. (2010) Plasma bile acids are not associated with energy metabolism in humans. Nutr Metab (Lond) 7: 73.
49. Brufau G, Stellaard F, Prado K, Bloks VW, Jonkers E, et al. (2010) Improved glycemic control with colesevelam treatment in patients with type 2 diabetes is not directly associated with changes in bile acid metabolism. Hepatology 52: 1455–1464.

Terawaki et al. Diabetology & Metabolic Syndrome 2013, 5:10
http://www.dmsjournal.com/content/5/1/10

DIABETOLOGY & METABOLIC SYNDROME

RESEARCH Open Access

The efficacy of incretin therapy in patients with type 2 diabetes undergoing hemodialysis

Yuichi Terawaki[1], Takashi Nomiyama[1*], Yuko Akehi[1], Hiromasa Takenoshita[1], Ryoko Nagaishi[1], Yoko Tsutsumi[1], Kunitaka Murase[1], Hisahiro Nagasako[1], Nobuya Hamanoue[1], Kaoru Sugimoto[1], Ayako Takada[1], Kenji Ito[2], Yasuhiro Abe[2], Yoshie Sasatomi[2], Satoru Ogahara[2], Hitoshi Nakashima[2], Takao Saito[2] and Toshihiko Yanase[1]

Abstract

Background: Although incretin therapy is clinically available in patients with type 2 diabetes undergoing hemodialysis, no study has yet examined whether incretin therapy is capable of maintaining glycemic control in this group of patients when switched from insulin therapy. In this study, we examined the efficacy of incretin therapy in patients with insulin-treated type 2 diabetes undergoing hemodialysis.

Methods: Ten type 2 diabetic patients undergoing hemodialysis received daily 0.3 mg liraglutide, 50 mg vildagliptin, and 6.25 mg alogliptin switched from insulin therapy on both the day of hemodialysis and the non-hemodialysis day. Blood glucose level was monitored by continuous glucose monitoring. After blood glucose control by insulin, patients were treated with three types of incretin therapy in a randomized crossover manner, with continuous glucose monitoring performed for each treatment.

Results: During treatment with incretin therapies, severe hyperglycemia and ketosis were not observed in any patients. Maximum blood glucose and mean blood glucose on the day of hemodialysis were significantly lower after treatment with liraglutide compared with treatment with alogliptin ($p < 0.05$), but not with vildagliptin. The standard deviation value, a marker of glucose fluctuation, on the non-hemodialysis day was significantly lower after treatment with liraglutide compared with treatment with insulin and alogliptin ($p < 0.05$), but not with vildagliptin. Furthermore, the duration of hyperglycemia was significantly shorter after treatment with liraglutide on both the hemodialysis and non-hemodialysis days compared with treatment with alogliptin ($p < 0.05$), but not with vildagliptin.

Conclusions: The data presented here suggest that patients with type 2 diabetes undergoing hemodialysis and insulin therapy could be treated with incretin therapy in some cases.

Keywords: Type 2 diabetes, Hemodialysis, Incretin therapy, CGM, Insulin therapy

Introduction

Diabetes is a multifactorial progressive disease accompanied by subsequent systematic vascular complications. Diabetic nephropathy is one of the most critical complications for diabetic patients because it can lead to severe renal failure, which requires treatment with hemodialysis (HD). Indeed, the major cause of the need for HD is diabetic nephropathy, and this has been the case in Japan since 1998. Controlling the blood glucose level of diabetic patients on HD is difficult, because of frequent hypoglycemia, restriction of the use of anti-diabetic agents, and instability of glucose, insulin, and drug metabolites between the day of HD and the non-HD day. However, strict glycemic control is important for the prognosis of diabetic patients with or without renal impairment [1]. Thus, additional effective and tolerable medications are urgently required for diabetic patients with renal impairment.

In recent years, medications that mimic or enhance incretin activity, such as glucagon-like peptide (GLP)-1 receptor agonists and dipeptidyl peptidase (DPP)-4 inhibitors, have emerged as important new treatments

* Correspondence: tnomiyama@fukuoka-u.ac.jp
[1]Department of Endocrinology and Diabetes Mellitus, School of Medicine, Fukuoka University, 7-45-1 Nanakuma, Jonan-ku, Fukuoka 814-0180, Japan
Full list of author information is available at the end of the article

for type 2 diabetes [2]. Incretins, such as GLP-1 and glucose-dependent insulinotropic polypeptide (GIP), are secreted after meals and act directly on pancreatic β cells to stimulate glucose-dependent insulin secretion. GLP-1 has multiple roles in the regulation of glucose metabolism, because it acts on pancreatic β cells and on other organs, including the brain, stomach, and vasculature [3]. However, intrinsic incretins are rapidly inactivated by DPP-4 [4], and as a result GLP-1 receptor agonists and DPP-4 inhibitors have been developed for the treatment of type 2 diabetes.

Incretin therapy is associated with additional benefits compared with other anti-diabetic agents. Firstly, incretin therapy does not induce hypoglycemia, because it controls blood glucose regulation by both insulin and glucagon secretion depending on the blood glucose level [5]. Additionally, incretin therapy may be able to protect pancreatic β cell function and volume, in contrast to sulfonylureas [6,7], and decrease blood glucose level without weight gain [8]. Recently, DPP-4 inhibitors have become one of the most frequently prescribed medications for type 2 diabetes in Japan, and we have previously reported the efficacy of a DPP-4 inhibitor, sitagliptin, in Japanese patients with type 2 diabetes [9]. Furthermore, some incretin therapies could potentially be used for blood glucose control in patients with type 2 diabetes who also have severe renal impairment [10].

According to the guidebook for chronic kidney disease (CKD) in Japan [11], DPP-4 inhibitors including 50 mg oral vildagliptin once-daily, 6.25 mg alogliptin, and the GLP-1 receptor agonist, liraglutide 0.3 mg injected once-daily, are available for treatment of patients with type 2 diabetes and end-stage renal disease (ESRD). However, there are no reports comparing the efficacy and safety of incretin therapies in diabetic patients on HD. In the present study, we examined the efficacy and safety of incretin therapy in patients with insulin-treated type 2 diabetes undergoing HD, using continuous glucose monitoring (CGM).

Subjects and methods

Subjects

Ten Japanese insulin-treated type 2 diabetic patients aged 34–83 years old and on HD were recruited for this study. Patients with a history of type 1 diabetes and diabetic ketoacidosis, severe impairment of intrinsic insulin secretion (serum C-peptide <2.0 ng/dL), requirement of high dose insulin injections (≥20 U/day), severe cardiac disease (New York Heart Association grade ≥III), or severe liver disease were excluded.

Baseline characteristics of the 10 patients are shown in Table 1. In this study, we measured glycated albumin (GA) as a marker of glycemic control, because GA is a more reliable glycemic control marker than glycated hemoglobin in patients with renal failure [12]. Baseline GA was 24.1 ± 1.5% and the mean duration of diabetes was 25.4 ± 2.3 years. Duration of HD was 4.1 ± 1.1 years. Serum-C peptide (S-CPR) was 6.7 ± 1.3 ng/mL, suggesting that patients still had intrinsic insulin secretion. The total dose of daily insulin injection was 11.6 ± 1.9 U/day. No patient had the anti-glutamic acid dehydrogenase (GAD) antibody or history of ketoacidosis. During hospitalization undergoing insulin or incretin therapy, all patients were treated with HD, thrice weekly for 4–5 hours with a bicarbonate dialysate containing 100 mg/dL of glucose. The calculated single-pool Kt/V [13] was 1.44 ± 0.09, suggesting sufficient efficacy of hemodialysis.

Table 1 Patient characteristics at baseline

Parameter	Value
n	10
Sex (male : female)	7:3
Age (years old)	62.9±4.3
Duration of diabetes (years)	25.4 ± 2.3
Duration of HD (years)	4.1±1.1
BMI (kg/m2)	23.0±1.5
Dose of insulin (U/day)	11.6±1.9
Glycated albumin (%) *	24.1 ± 1.5
S-CPR (ng/ml)	6.7 ± 1.3
spKTV	1.44 ± 0.09
Cre (mg/dl)	9.72±0.91
PTH (pg/ml)	88.0 ± 31.4
AST (U/l)	9.3 ± 1.1
ALT (U/l)	9.7 ± 1.3
gGTP (U/l)	16.9 ± 2.2
Total choresterol (mg/dl)	162.1 ± 8.1
Triglyceride (mg/dl)	120.1 ± 20.6
Blood glucose (mg/dl)	162.1 ± 8.1
Complications	
Macroangiopathy (– / +)	(6/4)
Neuropathy (– / +)	(0/10)
Retinopathy (– / +)	(0/10)

Values are means ± SEM or n. *n=9.

All patients provided written informed consent to participate. The study protocol was approved by the ethics committees at Fukuoka University Hospital. The study was performed in accordance with the ethical principles stated in the Declaration of Helsinki, 1964, amended in Edinburgh in 2000.

Methods

The present study design is shown in Figure 1. All patients were hospitalized and switched from insulin